THESIS FOR THE DEGREE OF DOCTOR OF PHILOSOPHY

# Formation of Mesoporous Materials and their use as Lipid Bilayer Supports

Maria Wallin


CHALMERS

Department of Chemical and Biological Engineering
CHALMERS UNIVERSITY OF TECHNOLOGY
Göteborg, Sweden 2014

Formation of Mesoporous Materials and their use as Lipid Bilayer Supports

Maria Wallin

ISBN: 978-91-7385-985-1

Doktorsavhandlingar vid Intuitionen för kemi- och bioteknik
Chalmers tekniska högskola
Serie Nr: 3666
ISSN: 0346-718X

Department of Chemical and Biological Engineering
Chalmers University of Technology
SE-412 96 Göteborg
Sweden
Telephone +46 (0)31-772 1000

Cover: SEM image showing the surface of a cubic mesoporous silica thin film. The highlighted schematic illustrates a lipid bilayer supported on a mesoporous surface.

Printed by:
Chalmers Reproservice
Göteborg, Sweden 2014

# Formation of Mesoporous Materials and their use as Lipid Bilayer Supports

Maria Wallin
Department of Chemical and Biological Engineering
Chalmers University of Technology

## ABSTRACT

Mesoporous materials have acquired great scientific interest in various applications; something that is largely due to that their properties, such as pore size, pore orientation, material composition and surface chemistry, can be controlled to a large extent. One idea, which has been investigated in this thesis, is to use mesoporous materials as supports for lipid bilayers and by doing so fabricate devices that mimic the cell membrane and at the same time has sufficient mechanical robustness for practical use. Such devices include biosensing and drug-delivery constructs where the pores are suggested to provide adequate environment for reconstituted sensing items, such as transmembrane proteins or serve as a reservoirs for therapeutics, and the pore-walls will provide stability to the bilayer.

The aim of this thesis was to form mesoporous silica and titania, and meso-ordered poly(ethylene glycol)diacrylate (PEG-DA) hydrogels, and to use these as supports for lipid bilayers. Both freely supported bilayers and covalently anchored lipid bilayers using "spacers", also called tethers, were examined. Moreover, the use of mesoporous silica and titania to enhance the detection of small analytes at low concentrations using quartz crystal microbalance with dissipation monitoring (QCM-D) was explored.

Mesoporous silica, titania and PEG-DA hydrogels were successfully synthesized using triblock copolymers or surfactants as structure directing agents. The results showed that bilayers were formed on mesoporous silica and that intact vesicle adsorption was obtained on titania, regardless of porosity. Homogeneously spread bilayers on PEG-DA bulk hydrogels were, however, difficult to form and resulted in that vesicles adsorbed intact or ruptured into lipid bilayer patches. Tethered lipid bilayers on amine-modified mesoporous silica were obtained by adsorbing tether containing vesicles on the surface and rupturing these using amphipathic α-helical (AH) peptides. The QCM-D signal-to-noise ratio was shown to be improved when mesoporous silica and titania were used as sensing surfaces, which was investigated by adsorbing different generations of dendrimers.

Based upon the results obtained in this thesis, mesoporous materials are considered to be promising supports for lipid bilayers in biosensing and drug delivery devices as well as to enhance the detection of small analytes at low concentration. Furthermore, the formed meso-ordered PEG-DA hydrogel particles have potential as drug delivery vehicles due to their narrow pore-size distribution, and soft and flexible structure.

**Keywords:** mesoporous silica, mesoporous titania, meso-ordered PEG-DA hydrogels, biosensing, lipid bilayers, tethered lipid bilayers, dendrimers, QCM-D, TEM

# List of publications

I Vesicle adsorption on mesoporous silica and titania
Maria Claesson*, Nam-Joon Cho, Curtis W. Frank and Martin Andersson
Langmuir, 2010, 26, 16630-16633

II Pore spanning lipid bilayers on mesoporous silica having varying pore size
Maria Claesson*, Rickard Frost, Sofia Svedhem and Martin Andersson
Langmuir, 2011, 27, 8974-8982

III Improved QCM-D signal-to-noise ratio using mesoporous silica and titania
Maria Claesson*, Akbar Ahmadi, Hoda M. Fathali and Martin Andersson
Sensors and Actuators B: Chemical, 2012, 166-167, 526-534

IV Meso-ordered soft hydrogels
Maria Claesson*, Kristin Engberg, Curtis W. Frank and Martin Andersson
Soft Matter, 2012, 8, 8149-8156

V PEG-based Hexosomes
Maria Wallin, Annika Altskär, Lars Nordstierna and Martin Andersson
Submitted to Journal of Physical Chemistry Letters

VI Tethered lipid bilayers on mesoporous silica
Maria Wallin, Jae Hyeok Choi, Seong Oh Kim, Nam-Joon Cho and Martin Andersson
Submitted to Journal of Colloid and Interface B

*In summer 2012 I got married and changed therefore my surname from Claesson to Wallin

# Contribution report

I Responsible for experimental work and for writing the manuscript.

II Responsible for experimental work except AFM analysis. Responsible for writing the manuscript.

III Responsible for performing and supervising experimental work. Responsible for writing the manuscript.

IV Responsible for experimental work and for writing the manuscript.

V Responsible for experimental work except NMR measurements and preparation of the embedded particles and replicas studied in TEM. Responsible for writing and submitting the manuscript.

VI Responsible for experimental work except AFM analysis. Responsible for writing and submitting the manuscript.

## Papers not included in this thesis

I Charged microcapsules for controlled release of hydrophobic actives Part II: Surface modification by LbL adsorption and lipid bilayer formation on properly anchored dispersant layers
Markus Andersson Trojer, Ye Li, Maria Wallin, Krister Holmberg and Magnus Nydén
Journal of Colloid and Interface Science, 2013, 409, 8-17

II Mesoporous silica thin films and particles prepared using monomeric, dimeric and trimeric cationic surfactants
Maria Wallin, Hasan Can Helvaci, Ali Reza Tehrani-Bagha and Martin Andersson
Submitted

# Table of contents

# Chapter 1

## Introduction

Mesoporous materials are defined as materials having pores with diameters between 2 and 50 nm [1]. The first mesoporous materials were synthesized in the early 70s [2-4], but did not receive their disserved attention until they were re-discovered by the researchers at Mobil Oil Cooperation in 1992 [5], who invented the Mobil Crystalline Materials, a.k.a. MCM-41. Since then, the research field of mesoporous materials has vastly grown and has caught interest in a wide range of applications including biomedicine [6-8], microelectronics [9, 10], sensing [11, 12], separation[13] and optics [14, 15]. The interest is driven by the unique properties of mesoporous materials such as high specific surface area, high content of surface-active groups and narrow pore size distribution along with the relatively straightforward means of controlling the material characteristics such as pore size, pore orientation and chemical composition. Mesoporous materials are generally synthesized using supramolecular assemblies of amphiphilic molecules forming templates of ordered structure, e.g. cubic, hexagonal or lamellar phases. Typically, inorganic oxides are synthesized such as silica, titania, alumina or mixed oxide. The inorganic material is cross-linked in the presence of the template and hardens and the structure-directing agent is then removed by pyrolysis or dissolution, using an appropriate solvent, resulting in the desired mesoporous material. A number of different parameters, including choice of precursor molecule, choice of amphiphilic molecule, presence of specific ions and condensation rate (mainly governed by the pH and temperature) influence the kind of mesoporous structure that is formed [16].

In this thesis, mesoporous materials have been formed with the aim of using them as supports for lipid bilayers in an effort to design robust cell mimicking surfaces, that can be applied for biosensing and drug delivery devices. Lipid bilayers are commonly used as basic model systems for living cell membranes and consist of mobile lipids organized in two layers. The advantage of using lipid bilayers in biomimicry is that these can be designed for specific applications by mixing lipids of choice or by reconstituting specific elements in the bilayer. For example, transmembrane proteins can be reconstituted for the use as sensing elements in biosensing devices or cell specific targeting groups can be imbedded for usage in drug-delivery applications [17-19]. The overall nature of lipid bilayers is that they are inert and impermeable to most substances [20]. Lipid bilayers are possible to form on different types of solid supports [21], however, up to

date few studies are found on the use of mesoporous materials as supports. Such supports are promising to use since the pores are suggested to provide an adequate environment for, example for reconstituted transmembrane proteins and to serve as a reservoir for drugs, and at the same time the walls between the pores can provide stability to the bilayer. In applications where the stability of the lipid bilayers is important it is advantageous to covalently anchor the bilayer to the supporting surface to increase the durability of the device. This is commonly achieved by the formation of tethered lipid bilayers to a surface [22], which will be further discussed in the thesis.

The materials in focus within this project have been mesoporous silica, titania and poly(ethylene glycol)diacrylate (PEG-DA). Mesoporous silica has potential in sensing and drug delivery devices and bone tissue regeneration whereas mesoporous titania is promising to use in sensing devices and osseointegration of implants [23, 24]. Meso-ordered PEG-DA hydrogels are biocompatible and are favorable for use in drug delivery applications and in the formation of synthetic tissue, such as the native cornea [25-27]. One aim of this thesis was to synthesize the before mentioned mesoporous metal oxides having varying pore size, pore geometry and when desired different surface functionalization's and to study the formation of lipid bilayers and tethered lipid bilayers on the formed mesoporous materials. One example of using mesoporous materials to enhance the signal-to-noise ratio of an acoustic sensing technique (QCM-D) is also included. Furthermore, results on the formation of meso-ordered PEG-DA bulk hydrogels and particles and the characterization of their microstructure are discussed. This thesis is divided into the following parts:

- Chapter 2 introduces the background for using mesoporous materials as supports for lipid bilayers in biosensing and drug delivery devices. This chapter also includes an introduction to the use of mesoporous materials to increase the signal-to-noise ratio when being used as a sensing surface in acoustic sensing. Moreover, the use of meso-ordered hydrogels in biomimicry applications is introduced.
- The used materials and methods are presented in Chapter 3.
- Chapter 4 deals with the obtained results of the formed mesoporous silica, titania and PEG-DA hydrogels.
- Chapter 5 discusses the adsorption of vesicles, with and without tethers, on mesoporous silica and titania as well as the influence of the pore size. Also, results of vesicle adsorption on PEG-DA hydrogels are included.
- A discussion on using mesoporous silica and titania to improve the signal-to-noise ratio of an acoustic sensing technique (QCM-D) is found in Chapter 6.
- In Chapter 7 conclusions and future work are presented.

# Chapter 2

## Background

In this chapter the use of mesoporous materials in sensing and drug delivery applications is motivated. More specifically, the use of the material as support for lipid bilayers, a delivery matrix for drugs and as a sensing surface is discussed.

### 2.1 Mesoporous supported lipid bilayers

Most living organisms consist of several cell types having various functions that together enable life on earth. A protective barrier, the cell membrane, which separates the interior from the exterior of the cell, surrounds each cell. The membrane has a complex structure consisting of a mixture of lipids (primarily phospholipids), proteins, glycoproteins, cholesterol and glycolipids. The cell membrane organizes and regulates enzyme activity, facilitates the transduction of information, supplies substrates for biosynthesis and for signal molecules and it even provides chemical and charge gradients that are established upon energy transfer between cells [28, 29]. These characteristics have resulted in that the cell membrane has received much attention in the development of novel drug delivery, catalysis and sensing devices [30, 31].

The lipids in the bilayer are fluid in both the lateral and the longitudinal plane and all the membrane constituents are mobile in the lateral plane, which increases the complexity of the system tremendously. This fluidity behavior was first described in the early 1970´s, which resulted in the fluid mosaic model [32]. However, today the theory is only true for simple descriptions of the living cell membrane, where some of its complexity is left out. In order to simplify the studies of cell membranes, basic model systems consisting of lipids (mainly phospholipids) that are organized in two layers having hydrophilic (polar) head groups on the outside and hydrophobic (nonpolar) alkyl chains on the inside are often used to mimic the membrane, as is illustrated in Fig. 1 [30, 33].

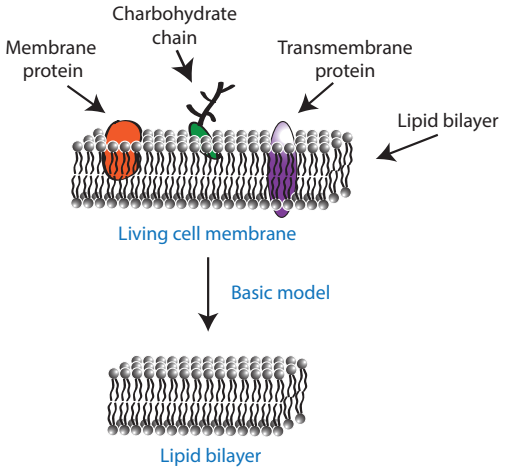


**Figure 1.** Illustration of a cell membrane and a basic model of the same, a lipid bilayer consisting only of lipids. adapted from [34].

Synthetic lipid membranes can be designed according to the application of interest by mixing lipids and cholesterol at certain ratios or by reconstituting proteins or other components of interest in the lipid matrix. Synthetic membranes have for example been used in the development of novel electrical and chemical biosensing devices using transmembrane proteins, such as ion channels, that can be utilized as sensing items [17, 18, 35]. In case of constructing functional biosensing devices, where lipid bilayers are used as hosts for proteins, the following requirements have to be fulfilled; the bilayer must be fluidic, provide available space below and above the membrane to avoid unwanted denaturation of proteins, and be free from defects to avoid formation of channels for ions and/or small molecules. Furthermore, the device should allow different kinds of detection and analysis as well as be reproducible, robust and stable over time [28].

Traditionally, membrane based biosensing devices, utilizing reconstituted transmembrane proteins as sensing items, have been designed either by having a lipid bilayer that is "hanging" freely between two hydrophobic walls (also called black lipid membranes)[36] or by having a lipid bilayer that is supported on a solid surface as is illustrated in Fig. 2 [37]. Both designs have advantages and disadvantages when it comes to constructing biosensing devices. The aperture spanning membrane design provides similar environments on both sides of the lipid bilayer; however the stability of the bilayer is relatively poor. The supporting lipid bilayer (SLB) design gives rise to opposite characteristics by providing stability to the lipid bilayer, but with the drawback of having dissimilar environment below and above the bilayer. In order to obtain fully functional transmembrane proteins in a bilayer and at the same time retain its stability over time it is important to construct a support that provides stability to a fluid lipid bilayer and at the same time provide enough space for the proteins. This is suggested to be obtained by combining the two traditional designs by having a mesoporous supported lipid bilayer (MSLB), where the walls of the pores will provide stability to the bilayer and the pore spanning part of the bilayer will give rise to an adequate environment and enough space below and above the bilayer, Fig. 2c.

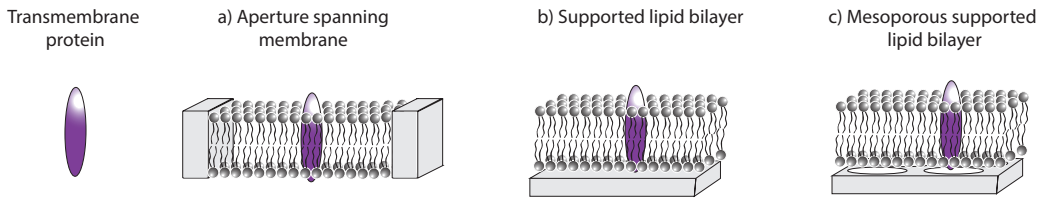


**Figure 2.** An illustration of the two traditonal designs of lipid bilayers used in biosensing devices (a) aperture spanning membrane, (b) supported lipid bilayer and our proposed design (c) mesoporous supported lipid bilayer.

MSLBs are furthermore useful in drug delivery applications, where the porous matrix could serve as a host for drugs and the lipid bilayer prevent premature drug release. In addition, target specific groups can be reconstituted in the bilayer to add sensitivity and selectivity to the device. These reconstituted groups are according to previous discussion also believed to gain from having a mesoporous support beneath the bilayer.

Lipid bilayers on porous material having a pore size of 20 nm - 4 μm have previously been investigated using florescent recovery after photo bleaching (FRAP) [38-41], atomic force microscopy (AFM) [42] and quartz crystal microbalance with dissipation monitoring (QCM-D) [43]. However, difficulties in forming pore spanning lipid bilayers on such supports and retaining it over time have been problematic without the use of chemical treatments of the surface or by adjusting the pH of the solution. To overcome these problems we propose to use mesoporous supports having pore sizes similar to the thickness of a lipid bilayer (5 nm [44]) The small size of the pores is believed to prevent the bilayer from entering the pores and also to provide a high stability. Pore spanning lipid bilayers on mesoporous silica particles have previously been shown to be possible to obtain. Such particles have been studied using for example, cryo-transmission electron microscopy (cryo-TEM) and small angle X-ray scattering (SAXS) [45-47]. However, the mechanism behind the formation of lipid bilayers on such supports needs to be further investigated.

The stability of the bilayer, when supported by mesoporous material, is suggested to increase if it is covalently attached to the support. An increased stability of the bilayer gives a more robust system, which prolongs the lifetime of the device. Bilayers are commonly anchored to a surface by the use of “spacers” having functional end-groups also referred to as tethers [17, 18]. These molecules provide a space between the bilayer and the support resulting in that denaturation of reconstituted items in the bilayer is avoided. Tethered lipid bilayers (TLBs) have been formed on different types of substrates using different techniques [48], however, up to date no study on the formation of lipid bilayer on mesoporous substrates via vesicle fusion using vesicles with reconstituted tethers has been performed. It is beneficial to form TLBs via tether containing vesicles since a better control of the distribution and amount of tethers is achieved compare to when tethers are anchored first followed by vesicle fusion.

## 2.2 Mesoporous materials used in sensing

Mesoporous materials are promising to use as sensing materials, especially in the detection of small molecules at low concentrations. For example, they can be utilized to increase the signal-to-noise ratio of the quartz crystal microbalance (QCM) technique. Here one takes advantage of the high specific surface area of the material and other tunable properties [49, 50]. By adjusting the characteristics of the material it can be optimized to detect molecules having a specific size and chemical composition. However, in order to utilize the high specific surface area, the detection is only achieved when the pore size is larger than the size of the analyte [51], see the illustration in Fig. 3. Previously, porous materials have been shown to enhance the QCM-D signal sensitivity and selectivity of molecules in gas phase. It was concluded that a larger surface area increased the ability for small molecules to interact with the surface, which was observed as an enhanced detection [50, 52, 53]. However, little is known about the improved sensitivity and selectivity using mesoporous materials in the detection of molecules in solution. Such systems are considered to be beneficial to use when screening, for example for toxic chemicals in nature or for molecules in a medical context.

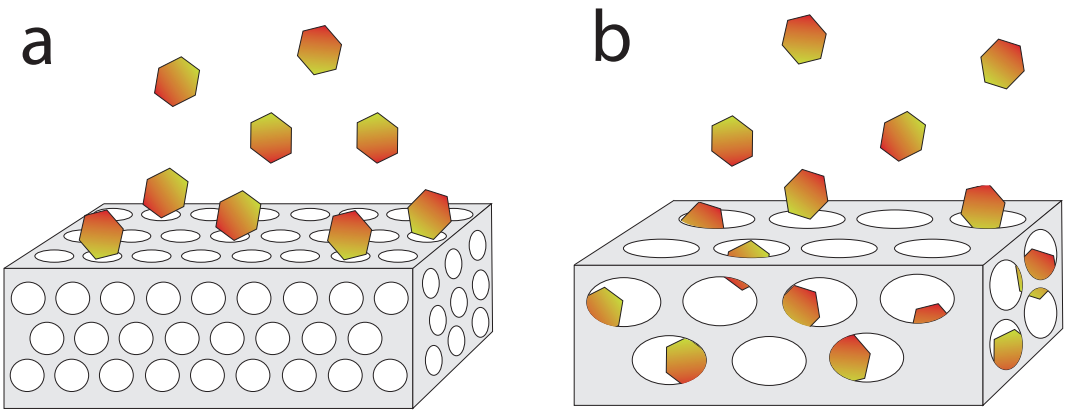


**Figure 3.** Illustration of cubic mesoporous material used as sensing surface, where analytes are shown to adsorb only on the outer surface of the material when their size is larger than the pores (a) and to adsorb on the surface within the pores when their size is smaller than the pores of the material (b).

## 2.3 Meso-ordered hydrogels

In recent years there has been a growing interest in the formation of hydrogels with controlled nanostructure. This is because such materials can provide increased mechanical integrity, greater diffusive transport and larger water transport than conventional hydrogels [54-57]. These improved properties give the material potential in a wide range of applications including drug-delivery, tissue scaffolds, artificial tissue, sensors, solar cells, electronics and separation membranes [58, 59].

One promising method to introduce nanostructure in hydrogels is to use a template consisting of a self-assembled structure directing agent onto which polymer segments adsorb and cross-link. The largest challenge with this approach is the thermodynamically driven phase separation typically occurring when monomers are converted to polymers. Phase separation results in poorly ordered hydrogel structures on much longer length scales than those obtained together with the templates. One solution to this phase separation problem which, has been explored by Guymons et al., is to rapidly cross-link the monomers in the presence of the templates utilizing photo polymerization [60].

The formation of meso-ordered hydrogels having a certain structure (i.e. cubic, hexagonal or lamellar) is largely dependent on the chemical nature of the polymers/monomers, the molecular length of the polymers/monomers and the properties of the structure directing agents. Also, the possibility of adjusting the shape of the meso-ordered hydrogels is of high interest to precisely design the material for a certain application. Ordered bulk hydrogels have for example potential in artificial tissue whereas ordered hydrogel particles are suggested to be useful in drug delivery applications.

# Chapter 3

## Materials and methods

In this chapter, surfactants and their properties are described together with the formation mechanism of mesoporous materials. Also, a brief introduction of the analytical techniques that have been used to study the pore size, pore geometry, film thickness and hydrophilicity of the materials will be presented. This is followed by a discussion about different cell membrane model systems and the techniques used to study vesicle adsorption on substrates, the lateral fluidity of lipids on solid supports and increase of the signal-to-noise ratio of the QCM-D signal.

### 3.1 Surfactants

Surface active molecules, commonly called surfactants, are amphiphilic molecules consisting of a hydrophobic (lyophilic) tail and a hydrophilic (lyophobic) head. The tail can be linear or branched, aliphatic, aromatic or mixture of both, short or long (typically between 8-16 carbons). The head can be nonionic, zwitterionic or ionic [61, 62]. Triblock copolymers composed of poly(ethylene oxide) EO and poly(propylene oxide) PO groups are also a type of amphiphile, which have similar properties as surfactants since the EO block is hydrophilic and the PO block is hydrophobic. The chemical structure of the surfactants and triblock copolymers used in this thesis are shown in Fig. 4.

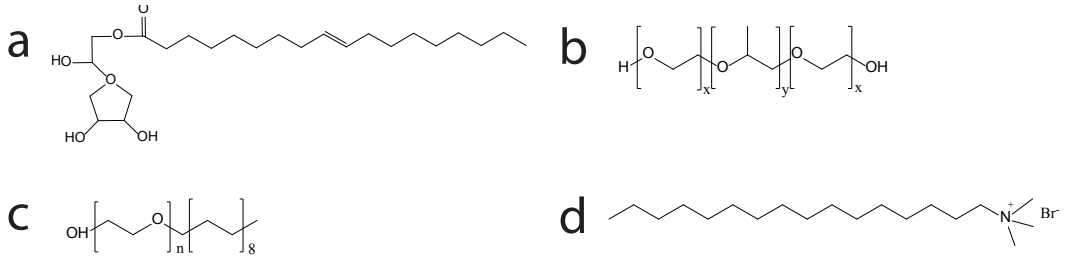


**Figure 4.** Molecular structure of the amphiphiles used in this thesis (a) sorbitan oleate (Span80) (b) poly(ethylene glycol)$_x$poly(propylene glycol)$_y$poly(ethylene glycol$_x$) ($EO_xPO_yEO_x$), (c) Polyoxyethylen(10) stearylether (BrijS10) and (d) cetyl trimethylammonium bromide (CTAB).

The high surface activity of surfactants results in that they preferably locate themselves at interfaces, for example at the air/water interface when dissolved in water. At a certain concentration (CMC) the surfactants start to aggregate into micelles, because of the hydrophobic effect [16]. With increasing concentration of surfactants more micelles are formed and at some point micelles come in direct contact. This inter-micellar state leads to aggregation of micelles into ordered structures, so called lyotropic liquid crystals (LLCs).

## 3.2 Lyotropic liquid crystals (LLCs)

LLCs have a long range order, however, are disordered at the short range molecular level. Depending on the molecular structure of the amphiphile, different LLCs can be formed; where singel-chain surfactants commonly aggregates into cubical or hexagonal structures and double-chain surfactants self-assembly into lamellar or revesed hexagonal structures [61]. In general, the interplay of the relaive bulkiness of the hydrophilic and hydrophobic domains of the amphiphile influences the LLCs formed. In order to predict the structure of the aggregate, a simplified molecular model of the surfactants can be used, which is based on geometrical parameters as is illustrated in Fig. 5 and Eq. 1 [61].

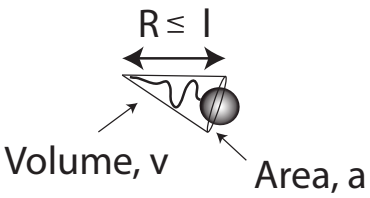


$$CPP = v/a \cdot l \qquad (1)$$

**Figure 5.** The preferred aggreagate structure of amphiphiles can be estimated using the critical packing parameter (CPP), which is based on the geometrical shape of the amphiphile.

In Fig 6., the relationship between the CPP and different self-assembly stuctures, including micells, cubic, hexagonal and lamellar structures, are illustrated.

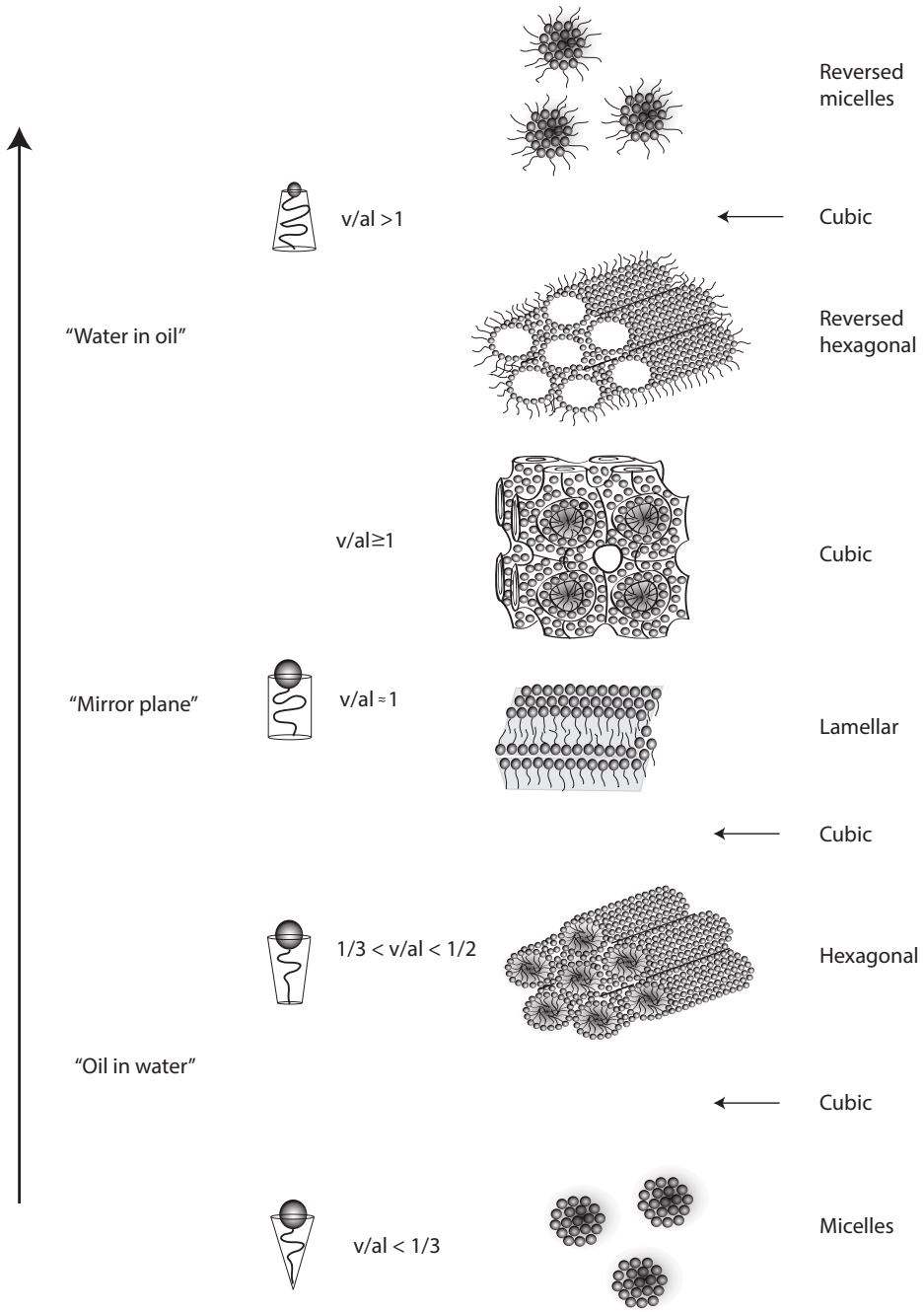


**Figure 6.** The relationship between the preferred aggregate structure and the critical packing parameter (CPP) of surfactant molecules. Redrawn from Holmberg et. al.; Surfactants and Polymers in Aqueous solution. 2nd ed [61].

Another factor that determines the LLCs that is beeing formed is the surfactant concentration. An increased surfactant concentration results in a change of LLC, typically from micellar, to hexagonal, to cubic structure etc [63]. Surfactants in LLCs of hexagonal, cubic and lamellar orientaion, are aligned in a bilayer with the hydrophobic tails pointing to each other leading to that the pore dimension or the distance between lamellar sheets corresponds to twice the length of the hydrophobic tail. For triblock copolymers the pore dimension or the distance between the lamellar sheets equals the length of the hydophobic block (PO) [16].

## 3.3 Mesoporous thin films

Mesoporous thin films are commonly formed following the solvent evaporation induced self-assembly (EISA) method. The formation protocol is relatively straight forward and simple to use and the obtained mesoporous films are continuous and often optically transparent [64]. The method utilizes amphiphilic substances, i.e. surfactants or triblock copolymers, having the possibility to form self-assemblies similar to LLCs as structure directing agents [64]. In principle, a LLC is formed together with the material precursor, which self-assembles and cross-links. Thin films are prepared by spin or dip coating using an ethanol solution of the reaction mixture. During the film preparation, ethanol evaporates inducing the self-assembly of surfactants or triblock copolymers together with precursors. This evaporation process gives rise to that the experimental condition changes continuously. Typically, the films are aged after the evaporation process for 24h followed by a heat treatment step resulting in removal of structure directing agents together with cross-linking and shrinkage of the mesoporous material, see Fig. 7. A unique feature of the formation of thin films is that the mesostructure aligns on a surface due to the presence of air/film and substrate/film interfaces [63].

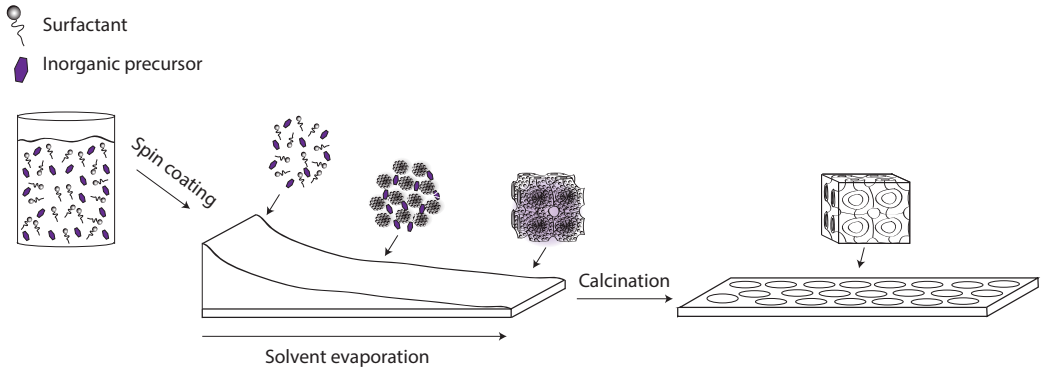


**Figure 7.** A schematic illustration on the formation of a cubic mesoporous thin film. In the figure a cubic thin film is formed on a surface by spin coating using a solution containing surfactant and precursors. The desired structure is formed by solvent evaporation resulting in self-assembly of surfactants and precursors. This is followed by removal of surfactants via calcination.

In the thesis, cubic mesoporous silica thin films having varying pore size and cubic and hexagonal titania thin films having similar pore size were synthesized. The different pore sizes were obtained by chancing the type of structure directing agents having different sizes. The synthesis and use of these mesoporous thin films are further described in **Paper I, II, III** and **VI**.

Thin films were prepared on quartz crystals (QCM-D, see Section 3.8) and glass slides by spin coating. The bicontinuous cubic structure was the preferred mesostructure for the lipid bilayer application due to that it gives rise to pore accessibility in all directions. This makes it possible to prepare thin films with pores facing the surface, which is essential in the study of the interaction between lipid bilayers and the pores matrix. Other structures, such as the hexagonal structure,

would be more problematic to use for this application since the structure consists of cylindrical tubes that most often are oriented parallel to the surface, which results in that no pores are facing the surface, see **Paper I, II** and **VI** [65]. In other applications, such as in the detection of small analytes at low concentration, where it is favorable to have a high specific surface area, both cubic and hexagonal surfaces are suggested to be useful. By comparing the adsorption of certain analytes on these surfaces it is possible to optimize the detection of a particular analyte. Also, the pore size of the material and the chemical composition of the material can be adjusted to enhance the detection of analytes, as is further discussed in **Paper III**.

## 3.4 Formation of meso-ordered hydrogels

Meso-ordered poly(ethylene glycol)diacrylate (PEG-DA) hydrogels were prepared by mixing precursors (PEG-DA) and structure directing agents (poly(ethylene glycol)$_x$-poly(propylene glycol)$_y$-poly(ethylene glycol)$_x$, $EO_xPO_yEO_x$) at different ratios followed by aging for 24h. The hydrogels were formed by cross-linking PEG-DA segments upon UV radiation. Finally, the LLC was removed by washing in ethanol and water. Prior to UV treatment, a photo initiator (2-Hydroxy-2-methylpropiophenone) was added to the precursor solution, which started a radical reaction resulting in cross-linking of PEG-DA segments and formation of meso-ordered hydrogels. The synthesis route is illustrated in Fig. 8. In the study, PEG-DA segments having different length and triblock copolymers having varying size and hydrophobicity were used to investigate the possibility of forming meso-ordered hydrogels, as further discussed in **Paper IV**.

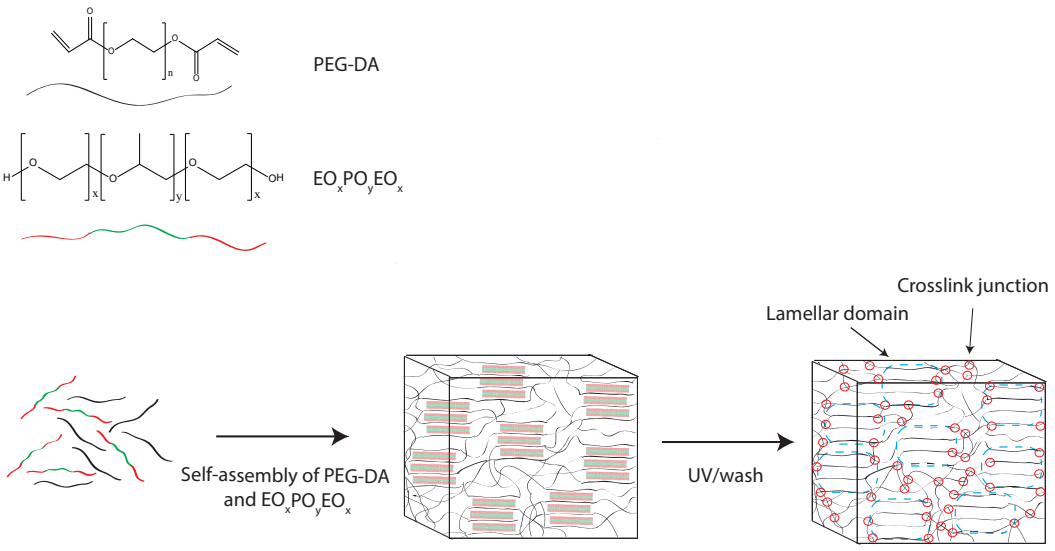


**Figure 8.** The formation of lamellar PEG-DA hydrogel is illustrated to be formed via self-assembly of poly(ethylene glycol)diacrylate (PEG-DA) and Pluronics ($EO_xPO_yEO_x$). The Pluronics constitute a template onto which PEG-DA cross-link using photo polarization (UV). In the final step the template is removed by washing resulting in a hydrogel containing lamellar domains.

## 3.5 Formation of PEG-based hexosomes

Hexagonally ordered PEG-DA hydrogel particles (PEG-based hexosomes) were synthesized in an inversed emulsion by mixing PEG-DA, photo initiator (2-Hydroxy-2-methylpropiophenone) and milli-Q water followed by slow addition of the solution into a nonpolar medium containing emulsifiers (surfactants) under constant stirring (**Paper V**). The PEG-DA segments were cross-linked upon UV radiation for 1h. Finally, the hydrogel particles were cleaned by liquid-liquid extraction, freeze drying and redispersed in water, as illustrated in Fig. 9. The emulsifier that was used is rather hydrophobic ($HLB_{Span80}$ = 4.3 [66, 67]) to obtain kinetically stable water in oil (w/o) emulsions.

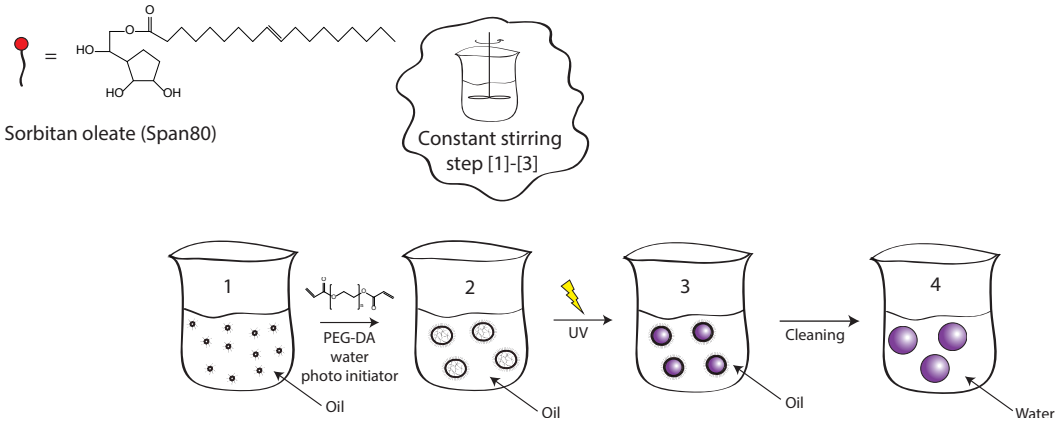


**Figure 9.** A schematic illustration on the procedure of forming PEG-DA hydrogel particles using a water in oil (w/o) emulsion. More precisely, a water solution containing PEG-DA and photo initiator was slowly poured into a solution containing emulsifier (Span80) and oil under constant stirring (1-2). PEG-DA was cross-linked via photo polymerization (UV) resulting in meso-ordered PEG-DA particles (3). Pure PEG-DA particles are obtained by removing oil and emulsifier (4).

## 3.6 Analytical techniques used for characterizing mesoporous materials and surfactants

The properties of the formed materials were characterized using transmission electron microscopy (TEM), cryogenic-TEM (cryo-TEM), scanning electron microscopy (SEM), polarized light microscopy (PLM), nitrogen adsorption-desorption measurements, small angle X-ray scattering (SAXS), contact angle measurements and nuclear magnetic resonance (NMR) spectroscopy.

**TEM** and **SEM** are both electron microscopy techniques, in which electrons are used to visualize materials at high magnification. These methods are based on accelerating electrons at high voltages (TEM, up to 400 kV; SEM, 1-50 kV) in a vacuum column onto the sample. Interactions between the electrons and the sample of interest occur resulting in various signals, which are monitored using different detectors. The electrons show similar characteristics as the light in optical microscopes; however their wavelength is shorter, which results in higher resolutions. Using TEM a resolution of a few Ångströms (Å) can be obtained and using SEM structures having a size of a few nanometers (nm) can be visualized. The main difference between the two techniques is the interaction between the electrons and the sample. In the TEM, electrons are transmitted through the sample and in the SEM electrons are scanned over the sample surface. This results in that TEM only allows characterization of thin samples (ca 100 nm) whereas SEM analysis is independent of the thickness of the sample. As a consequence, different information can be obtained for the two techniques. TEM gives structural information, such as pore size and pore geometry and in the SEM information of for example porosity, morphology and size of the sample is given. In the present thesis, TEM was used to visualize the structure and pore size of the mesoporous material and SEM was used to measure the thickness and study the pore orientation of the obtained mesoporous thin films. TEM analysis was carried out on a JEM-1200 EX II TEM operated at 120 kV (Jeol, Tokyo, Japan) and the SEM used was a Leo Ultra 55 FEG SEM (Leo Electron Microscopy, Cambridge, UK). Prior to analysis, TEM specimens were prepared by scratching off mesoporous thin films from coated glass slides followed by dispersion in Ethanol (proof 200) and then by sonication for 2 min. A small amount of the dispersion was applied on TEM grids (Lacey Formvar/Carbon 300 mesh, Caspilor, Sweden) and then degassed in air. SEM samples were prepared by rinsing in Ethanol (proof 200), milli-Q water and UV treated, followed by sputtering with gold (20 nm) in an ion sputter JFC-1100E (JEOL, Tokyo, Japan). TEM on fully swollen bulk hydrogels and hydrogel particles in milli-Q water was furthermore performed using a LEO 706E (LEO Electron Microscopy Ltd., Cambridge, England) at 80 kV accelerating voltage. Prior to analysis, replicas of the samples were prepared according to the freeze etching method for the bulk hydrogels and the mica sandwich technique for the hydrogel particles [68]. TEM micrographs were also taken on agarose embedded particles.

**PLM** is based on a conventional light microscope equipped with two polarized filters. The technique is used to visualize anisotropic order in a material by studying the scattered polarized light, so called birefringence. Two structures that show birefringence are the lamellar (L) and hexagonal (H) structure which are recognized as oily streaks and as non-geometrical patterns, respectively [69]. The light microscope used was a Zeiss Axiovert light microscope (Göttinge, Germany) (10x objective).

**Nitrogen adsorption-desorption** analysis is mainly used to collect information about the specific surface area and pore size distribution of a material, following the BET (Brunauer, Emmett and Teller) and BJH (Barrett, Joyner and Halenda) method, respectively [70, 71]. The technique is based on measuring the adsorption/desorption of nitrogen on a sample under controlled pressure and temperature using liquid nitrogen. Upon increased partial pressure of nitrogen, a larger amount of gas molecules can be adsorbed on the sample and vice versa. The increase in pressure is preceded until the point of condensation of adsorbed gas is reached inside the pores. From this the equilibrium pressure is measured and used in the calculation of the adsorbed/desorbed amount of gas molecules in the sample using universal gas laws. In this thesis, nitrogen adsorption-desorption analysis was used as a complementary technique to TEM by measuring the diameter of the pores using the BJH method and also to measure the surface area of mesoporous material according to the BET method [70, 71]. The analysis was performed on a Micrometrics Tristar (Norcross, GA). The samples were prepared by scratching off mesoporous coated glass slides (10 · 20 cm) followed by degassing in a vacuum oven at 250 °C for 3h.

**SAXS** is an analysis method that can be used in the characterization of the intermolecular structure, such as to identify if the mesostructure is lamellar, cubic or hexagonal. The technique provides information about regularities, order and periodicity in a material at a length scale of 1-100 nm. Furthermore, information about the pore size or the distance between two lamellar sheets can be obtained by the position of the Bragg peaks appearing in a graph where the intensity (I) is plotted against the scattering angle (θ). The peaks are shifted to larger angles (θ) for materials having shorter repetitive distances. The principle behind the technique is to measure the interference of X-ray (photons) with a sample at small angles (1-10°). The difference in angle of the incident beam, having a certain wavelength, and the out coming beam, containing scattering X-rays, are compared and used in the calculation of the intermolecular structure, according to Bragg's law, which is shown in Eq. 2.

$$n\lambda = 2d\sin\theta \qquad (2)$$

where n is an integer (path difference), λ is the wavelength of the incoming beam, d is the spacing between the parallel crystal planes and θ describes the angle between the incoming and the reflected beams and the diffracting crystal plane as illustrated in Fig. 10.

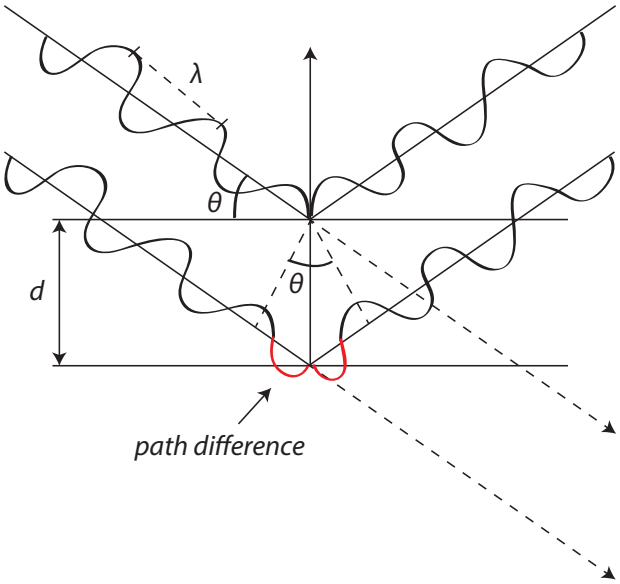


**Figure 10.** Schematic illustrates x-ray diffraction according to Braggs law.

In this thesis, SAXS data was obtained using a synchrotron source. Synchrotron measurements were performed on beamline I711 and I911 at the Maxlab synchrotron facility (Lund, Sweden) and on beamline 1-4 at the Stanford Synchrotron Radiation Light source (SSRL, Stanford, CA).

**Contact angle measurements** provide information about the interfacial free energy of a surface by measuring the equilibrium contact angle (θ) between a surface and a liquid. This is performed by placing a droplet on a surface and measure the angle (θ) between the two using a microscope fitted with a goniometer eyepiece/camera. The technique is very sensitive to contaminations, impurities and topography of a surface. Hydrophilic surfaces correspond to angles less than 90°, and hydrophobic surfaces correspond to a contact angles above 90°. The surface free energy is calculated according to Young's equation, see Eq. 3.

$$\gamma_{SV} = \gamma_{SL} + \gamma_{LV}\cos(\theta)_c \qquad (3)$$

where $\gamma_{SL}$, $\gamma_{LV}$, and $\gamma_{SV}$ are the interfacial tensions between the solid and the liquid, the liquid and the vapor, and the solid and the vapor respectively, as is illustrated in Fig. 11 [61].

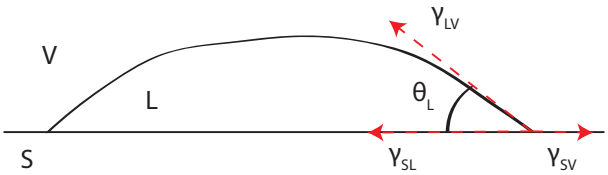


**Figure 11.** An illustration of the interfacial tension between solid, liquid and air according to Young's equation.

The contact angle measurements were performed using a dynamic absorption tester (DAT 1100, FIBRO systems AB, Sweden) on nonporous and mesoporous silica surfaces. Prior to analysis, the surfaces were rinsed in SDS for 15 min, in milli-Q water for 5 min, dried using nitrogen gas and then UV treated for 15 min.

**NMR** The molecular structure of the synthesized PEG-DA and the removal of Span80 (LLC) from the hydrogel particles were analyzed using a Varian MR 400 spectrometer (Palo Alto, CA). Complementary $^2$H spectra were studied to analyze the presence of meso-order within the hydrogel particles by swelling the particles in $D_2O$ prior to analysis followed by studying the quadrupolar splitting of the $D_2O$ signal [72]. The $^2$H measurements were carried out using a Bruker Avance 600 spectrometer (Bruker, Karlsruhe, Germany) equipped with a Diff30 probe with a 5 mm RF insert with $^1$H and $^2$H coils. All NMR experiments in this work were carried out at 25 °C. For the spectral analysis, the software program MestReNova version 8.1.2 (Mestrelab Research, Santiago de Compostela, Spain) was used.

## 3.7 Model systems for cell membranes

The living cell membrane is commonly modeled by liposomes [73], supported lipid bilayers (SLBs) [21, 74, 75] or Langmuir-Blodgett films (LB-model) [76]. A liposome, also called a lipid vesicle, is a simplified model of the living cell membrane, which consists of one type or a mixture of nonpolar and polar lipids and/or other components such as cholesterol and membrane proteins. Unilamellar vesicles (vesicles consisting of one bilayer) having different sizes can be prepared by mixing components of interest followed by extrusion using polycarbonate membranes with a well-defined pore size [77]. The advantages of using vesicles as a model system for the cell membrane is that a suitable environment for reconstituting proteins and other components can be provided due to that the interior and the exterior of the vesicle are similar to the living cell membrane. However, the model is limited concerning detection methods to evaluate changes in the amount of substances or charges in the interior of the vesicle. This detection problem can be solved by having a bilayer that is supported on a solid support, which is connected to a detection system. Supported lipid bilayers can either be constructed by adsorbing vesicles that ruptures on a surface at a critical vesicle concentration, which results in the formation of lipid bilayers (SLB model), or by forming a monolayer of lipids on a support onto which another monolayer is placed, according to the LB-method. Drawbacks of having a solid support underneath the membrane is that proteins and other components might lose their mobility due to interactions with the support as discussed in Chapter 2. To avoid these unwanted interactions between the proteins and the support, lipid bilayers have been formed on polymer cushions or on tether molecules that are used as a "spacers" between the bilayer and the surface [22, 78, 79].

In this thesis, the SLB model was utilized using three different types of vesicles, one only containing phospholipids (1-palmitoyl-2-oleoyl-sn-glycero-3-phosphocholine, POPC), one consisting of POPC and 1-2 wt% of the fluorescent lipid probe Rhodamine-DHPE (Lissamine™ rhodamine B 1,2-dihexadecanoyl-sn-glycerol-3-phosphatidylethanolamine) and one type of vesicle consisting of POPC lipids mixed with 2 wt% DSPE-$PEG_{2000}$-NHS (1,2-distearoyl-sn-glycero-3-phosphoethanolamine-N-[maleimide(polyethylene glycol)-2000]) used as tether, as is shown in Fig. 12.

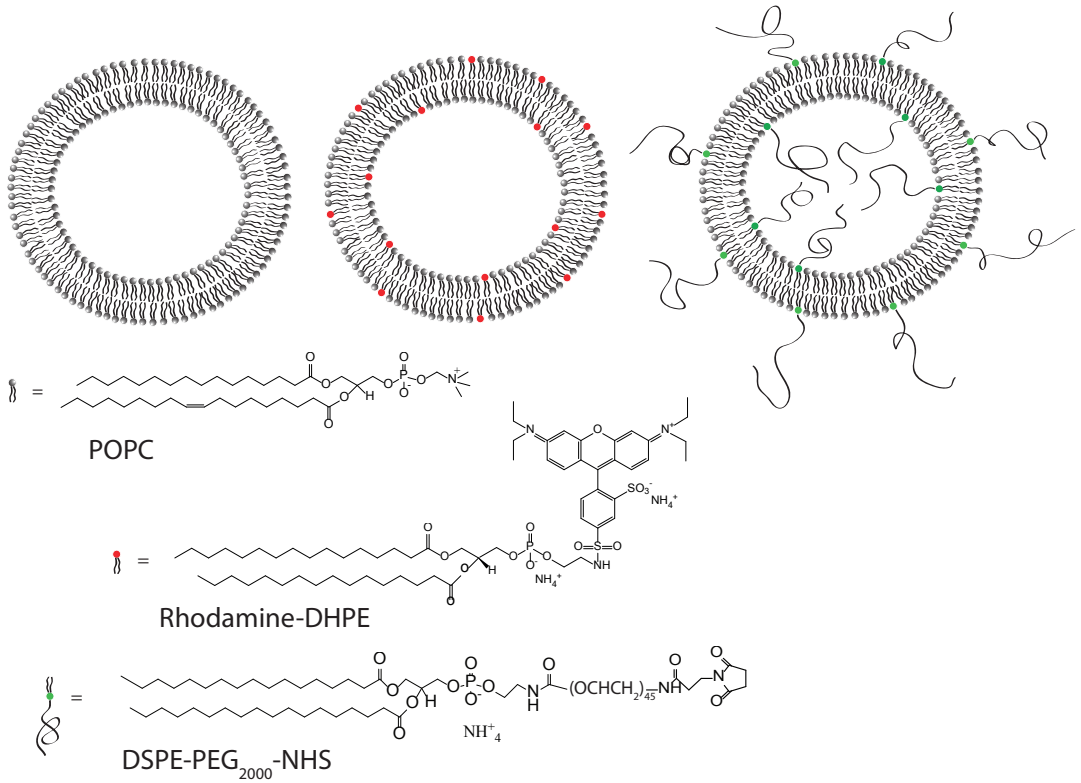


**Figure 12.** A schematic showing vesicles containing 1-palmitoyl-2-oleoyl-sn-glycero-3-phosphocholine (POPC) lipids (left), a mixture of POPC and Lissamine™ rhodamine B 1,2-dihexadecanoyl-sn-glycerol-3-phosphatidylethanolamine1,2-distearoyl-sn-glycero-3-phosphoethanolamine-N-[maleimide(polyethylene glycol-2000 (Rhodamine-DHPE) lipids (middle) as well as a mixture of POPC lipids and (DSPE-$PEG_{2000}$NHS) (right).

Vesicle adsorption of plain POPC vesicles and POPC vesicles containing tethers were investigated on nonporous and mesoporous silica and titania as well as on PEG-DA hydrogels. The fluorescently labeled lipids were used to verify the presence of lipid bilayers on a surface and to study the fluidity of lipids in the bilayer. The vesicles were prepared by mixing lipids in water/buffer followed by extrusion using a mini-extruder (Avanti Mini-Extruder, Avanti polar lipids, Alabaster, AL) through a polycarbonate membrane having pore sizes of 100, 50 and 30 nm; 21 times for each membrane.

## 3.8 Analytical techniques used to study bilayers and for detection of small analytes

The interaction between mesoporous materials or PEG-DA hydrogels and vesicles was investigated using quartz crystal microbalance with dissipation monitoring (QCM-D) and atomic force microscopy (AFM) and the fluidity of lipids in the bilayer was studied using fluorescence recovery after photo bleaching (FRAP). QCM-D was furthermore used to study the improvement of the signal-to-noise ratio when mesoporous thin films were used as sensing material. Prior to analysis, the size of the vesicles and dendrimers, which were used to investigate the mesoporous surfaces, was measured using dynamic light scattering (DLS). DLS was also used to measure the average size of the synthesized hydrogel particles.

**QCM-D** is a surface sensitive technique that measures adsorption of molecules in real time on an oscillating quartz crystal. The method provides information regarding the adsorbed mass (including acoustically coupled water) and the elastic and viscoelastic properties of the adsorbed layer. The mass is related to changes in resonance frequency (Δf) of the piezoelectric quartz crystal and the viscoelastic properties are related to changes in the damping of the crystal, referred to as changes in dissipation (ΔD) as is illustrated in Fig. 13.

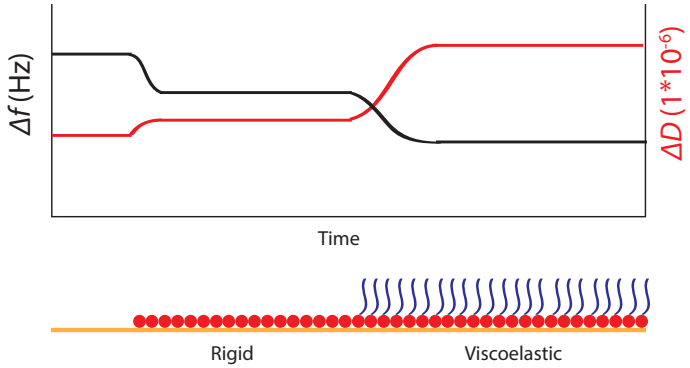


**Figure 13.** An illustration of the QCM-D measuring technique. Typical shifts in Δf and ΔD are shown in QCM-D for the adsorption of a rigid and a viscoelastic layer, respectively.

For rigid films, the Sauerbrey equation can be used to calculate the mass of the adsorbed layer, according to Eq. (4).

$$\Delta m = - C \cdot \Delta f_{norm} \qquad (4)$$

where C is the mass sensitive constant, C = 17.7 ng·cm$^{-2}$·Hz$^{-1}$ for crystals with a fundamental resonance frequency of 5 MHz and $\Delta f_{norm} = \Delta f_n/n$, with n being the overtone (1, 3 etc.) [80, 81]. QCM-D was used to investigate the kinetics of the lipid bilayer formation by adsorbing vesicles on mesoporous coated quartz crystals. In Figure 14, a QCM-D crystal coated with cubic mesoporous material is illustrated.

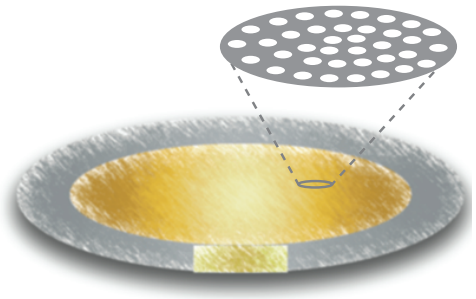

**Figure 14.** Schematic shows a quartz crystal sensor coated with cubic mesoporous material.

The formation of lipid bilayers are shown in QCM-D data to be formed via adsorption of vesicles on the crystal surface, seen as a decrease in Δf and an increase in ΔD, until a certain concentration of vesicles are reached on the surface, so called the critical concentration of vesicles. At this point, vesicles start to rupture and spread on the surface resulting in release of water from the interior of the vesicles, which is observed in the QCM-D data as an increase in Δf and decrease in ΔD. At certain conditions, lipid bilayers can also be formed via immediate rupturing of the vesicles upon contact with the surface. The final frequency ($f_{final}$) and dissipation ($D_{final}$) shifts for lipid bilayers typically equals ~26 Hz and~ $0.1 \cdot 10^{-6}$ respectively, see **Paper I** and **II** [82]. In addition, QCM-D results for the attachment of lipid bilayers to a surface using tether molecules are presented and discussed in **Paper VI**. The pore volume of mesoporous silica and titania was also investigated using QCM-D by measuring the trapped water within the pores. This was measured by exchanging milli-Q water ($H_2O$) with pure deuterium oxide ($D_2O$), were Δf can be used to calculate the pore-volume that is accessible for water, **Paper III**. The possibility of enhancing the signal-to-noise ratio of the QCM-D signal was evaluated by adsorbing four different generations of dendrimers on mesoporous and nonporous silica and titania coated QCM-D crystals as is further discussed in **Paper III**. Dendrimers are spherical polymers with well-defined sizes. The smallest dendrimres are obtained at the lowest generation and vice versa. Since the size is well-defined, a good correlation between the size of the pores and the size of the dendrimers can be obtained when these are adsorbed on mesoporous materials.

Prior to analysis, the QCM-D crystals (14 mm, Q-sense AB, Gothenburg, Sweden) were rinsed in 10 mM SDS for 15 min, milli-Q water for 5 min, dried using nitrogen gas and then UV-ozone treated for 15 min.

**FRAP** analysis can be used to measure the lateral mobility of lipids in a bilayer. This was performed by forming a lipid membrane including 1-2 wt% of fluorophores on the surface followed by quickly focusing an intense laser on a small region of a surface. The fluorophores that are exposed to the laser will be irreversibly photo chemically bleached. As discussed previously, lipid bilayers contain mobile lipids, which accordingly imply that the bleached fluorophores gradually will mix with the unbleached fluorophores with time, if a fluid bilayer is present, as is shown in Fig. 15.

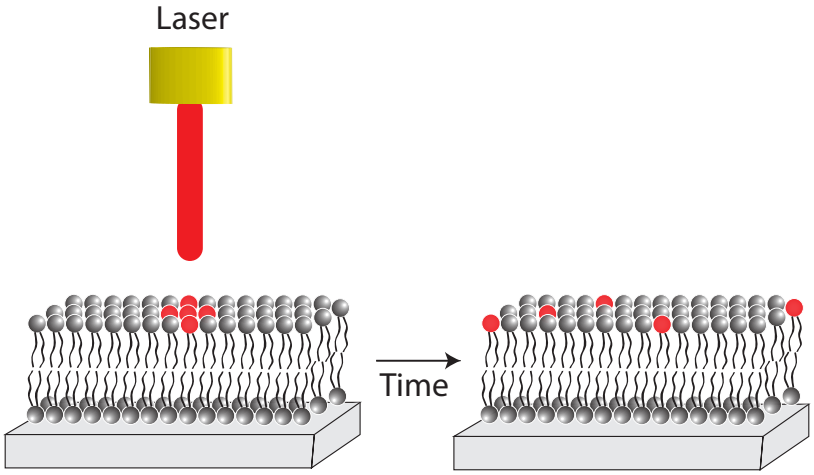


**Figure 15.** Illustration of a FRAP measurement where fluorophores in a lipid bilayer are bleached and gradually mixed with unbleached lipids with time.

In case vesicles are adsorbed intact on a surface, no recovery of the bleached spot will occur. The time it takes for the bleached region to be recovered is then used to calculate the diffusion coefficient of lipids (D), according to Eq. 5.

$$D = 0.224\ (w^2/\tau_{1/2}) \qquad (5)$$

where w describes the radius of the bleached area and $\tau_{1/2}$ is the half time of the recovery [31, 83]. In this work, FRAP was used to verify the presence of lipid bilayers and to investigate the impact the surface had on the fluidity of the lipids. FRAP measurements were carried out on coated glass surfaces on a FRAP setup that was based on an inverted Nikon Eclipse Ti-E microscope (Nikon Corporation, Tokyo, Japan) equipped with an EMCCD Andor iXon camera (Andor Technology, Belfast, Northern Ireland) or on an upright Axioplan 2 microscope (Zeiss, Germany) equipped with an AxioCam (Zeiss, Germany). Prior to analysis the surfaces were rinsed according to the protocol used for QCM-D.

**AFM** is used to measure the topography of a surface in a dry or a liquid environment either by having a cantilever that is scanned in contact, not in contact or tapped on the surface (contact or tapping mode) and simultaneously measure the interactions. The interaction measurements are performed by focusing a laser on the cantilever tip and continuously detect the deflection as it is exposed to upon interaction with the surface, see Fig 16.

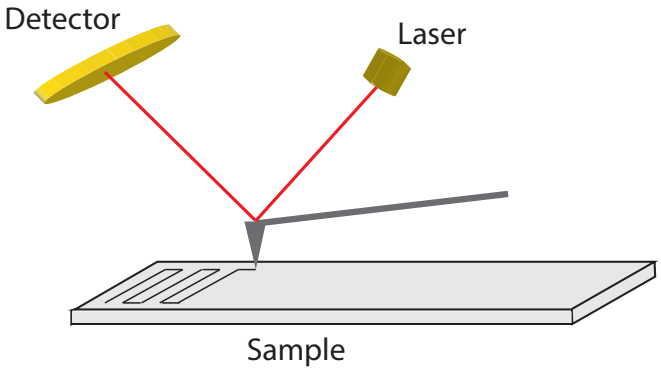


**Figure 16.** Schematic illustration of an AFM set-up. The surface roughness is analyzed by recording the vertical movement of a cantilever while it scans over a surface by the use of laser light.

Furthermore, the presence of a lipid bilayer on a support can be observed by performing force spectroscopy measurements. This is performed by measuring the force versus the distance between the tip and the sample at a fixed lateral position. Intermolecular forces between the two can be measured and used to determine the length or thickness of an object. The mobility of lipid bilayers can be visualized by performing square test on the bilayer by destroying the bilayer and then study the recovery over time.

The cantilever is usually made from silicon or silicon nitride and has a spring constant between 0.01 and 100 N/m. In this work, contact and tapping mode AFM were applied at a constant force in a liquid environment [84, 85]. The AFM was used to evaluate the homogeneity and continuity of supported lipid bilayers and tethered lipid bilayers on the various surfaces as well as comparing the interaction between vesicles on mesoporous and nonporous silica. Square tests were performed on the tethered lipid bilayer to measure the thickness of the bilayer and to investigate the mobility of the lipids in the tethered lipid bilayer by studying the recovery of the square with time. The AFM measurements were performed in liquid using a PicoSPM microscope (Agilent/Molecular Imaging Inc., Palo Alto, CA) or a NX-Bio (Park Systems, South Korea). Prior to analysis the surfaces were rinsed following the same protocol as described for the QCM-D, see above.

**DLS** is used to determine the size of macromolecules or colloidal particles in solution by measuring the scattered light from a small given volume. In this small volume the amount of particles changes upon Brownian motion, which results in fluctuations in the scattered light. The Brownian motion is described as a stochastic process caused by collisions between particles and the surrounding medium. DLS is performed by directing a laser on the sample and then detect the scattered light caused by the particles in the solution. Due to Brownian motion, the intensity of the scattered light fluctuates with time, which is recorded and used to determine the size of the particles. A large particle has a slower motion than a small particle resulting in smaller fluctuations in the scattered light [86]. In this work, DLS was used to measure the size and size distribution of the extruded vesicles, the different generations of dendrimers and the hydrogel particles using a Zetasizer nano-ZS (Malvern instruments, Worcestershire, UK) or 90 Plus Particle Size analyzer (Brookhaven Instruments, Holtsville, NY, USA). The data for the estimated size of the vesicles were collected from z-average values.

# Chapter 4

## Characterization of meso-ordered material

The results from the synthesized mesoporous silica and titania material as well as the formation of meso-ordered PEG-DA bulk hydrogels and particles are discussed in the following chapter.

### 4.1 Mesoporous silica and titania thin films

Cubic mesoporous silica and cubic and hexagonal mesoporous titania thin films were successfully formed on glass slides and AT-cut QCM-D sensor crystals using the solvent evaporation method, according to TEM micrographs shown in Fig. 17. The pore size of the synthesized silica materials were measured directly from TEM micrographs to be about 5-6 nm, 3-4 nm and 2-3 nm using P123, BrijS10 and CTAB, respectively, as structure directing agents and about 4 nm for cubic and hexagonal mesoporous titania using P123 as a structure directing agent. These values correspond well with sizes obtained in previous studies [65, 87, 88].

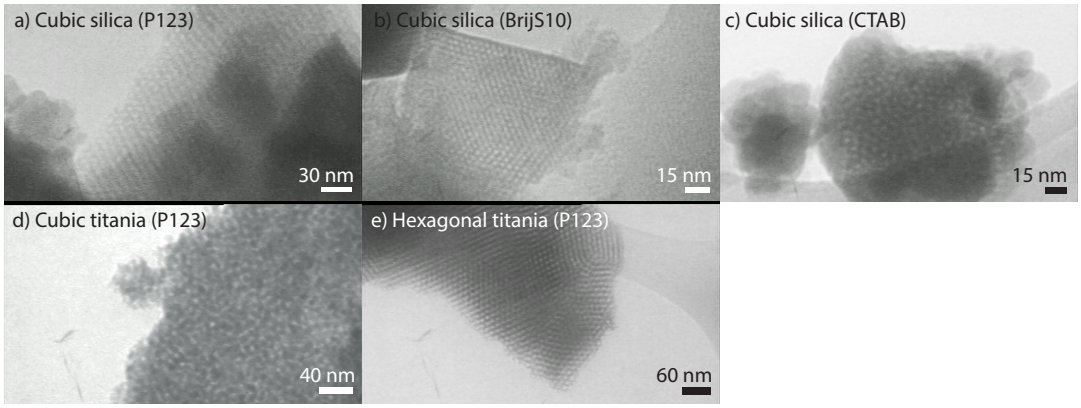


**Figure 17.** TEM micrographs showing cubic mesoporous silica with different pore sizes (a)-(c). In (d) cubic and (e) hexagonal mesoporous titania are shown. The pore size was varied by the choice of structure directing agent (P123, BrijS10 or CTAB) and the meso-ordered structure was tuned by the amount of structure directing agent.

The size of the pores were also calculated using nitrogen adsorption-desorption measurements (BJH) to be 5.2 nm for mesoporous silica prepared using P123, 2.7 nm using BrijS10 and 2.4 nm using CTAB and for hexagonal and cubic mesoporous titania a pore diameter of 3.6 nm and 4.1 nm, respectively was obtained when P123 was used as structure directing agent. These values differed

from the measured pore sizes in TEM micrographs, which is believed to be caused by the co-existence of micro- and mesopores in the material, which has an impact on the nitrogen adsorption-desorption results. Moreover, for the smaller pores the lowest pressure used might not be low enough to reach full condensation of nitrogen gas [70, 71, 87].

SAXS measurements gave at least one Bragg peak for each material, which confirmed that the materials were ordered, as is shown in Fig. 18. The first Bragg peak appeared at θ ~ 0.6, θ ~ 1.25 and θ ~ 1.6 for mesoporous silica synthesized using P123, BrijS10 and CTAB as structure directing agent, respectively and at θ ~ 0.4 and θ ~ 0.3, respectively, for cubic and hexagonal mesoporous titania templated with P123 as structure directing agent. A Bragg peak that is shifted to larger angles corresponds to shorter repetitive distance within the material.

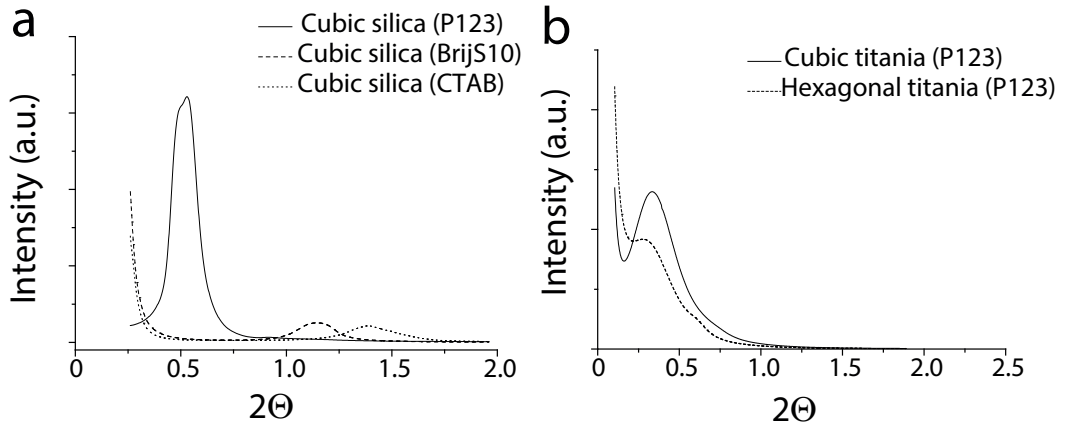


**Figure 18.** SAXS results shown as the intensity (I) as a function of the angle (2θ) of (a) cubic mesoporous silica prepared using different template agents (P123, BrijS10 and CTAB) and (b) cubic and hexagonal titania prepared using P123 as templating agent.

In figure 19, SEM micrographs showing that hexagonal thin films consisted of worm-like tubes, having pores on the ends that are lying parallel to the surface and that cubic thin films have pores that are accessible also from the surface.

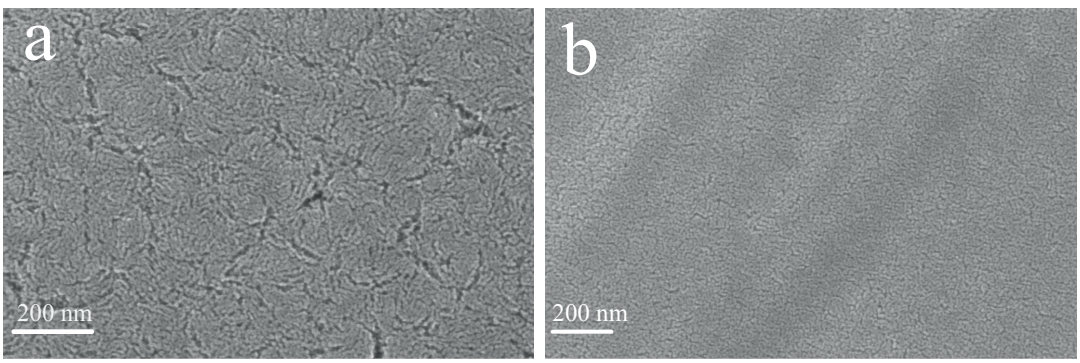


**Figure 19.** SEM micrographs showing (a) a hexagonal and (b) a cubic mesoporous titania surface.

The thicknesses of the spin coated (4000 rpm) thin films varied between 160 and 350 nm for the different mesoporous materials, which was measured from SEM micrographs obtained from cross-sections of the film, as seen in Fig 20.

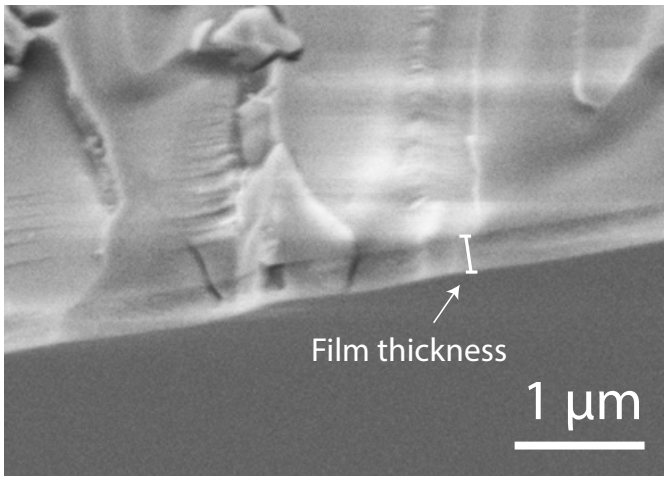


**Figure 20.** A SEM micrograph showing a typical cross section of a thin film formed using a spin rate of 4000 rpm. In this figure, mesoporous silica prepared using P123 as a template is shown.

From QCM-D measurements, the pore volume of the different mesoporous thin films was retrieved by studying the change in Δf, that occurred when $H_2O$ was exchanged with $D_2O$, see Fig. 21. $H_2O$ and $D_2O$ are believed to adsorb similarly to all tested surfaces due to their comparable size and chemical composition. However, their different pH and hydrogen binding capacity probably have an impact on the final results. In QCM-D, the change in ΔD was similar on all surfaces including the nonporous surface, which was believed to correspond to bulk effects. Accordingly, Sauerbreys equation could be used to calculate the areal mass/film thickness. The obtained pore volume includes both micro and meso pores, that are accessible for water [87].

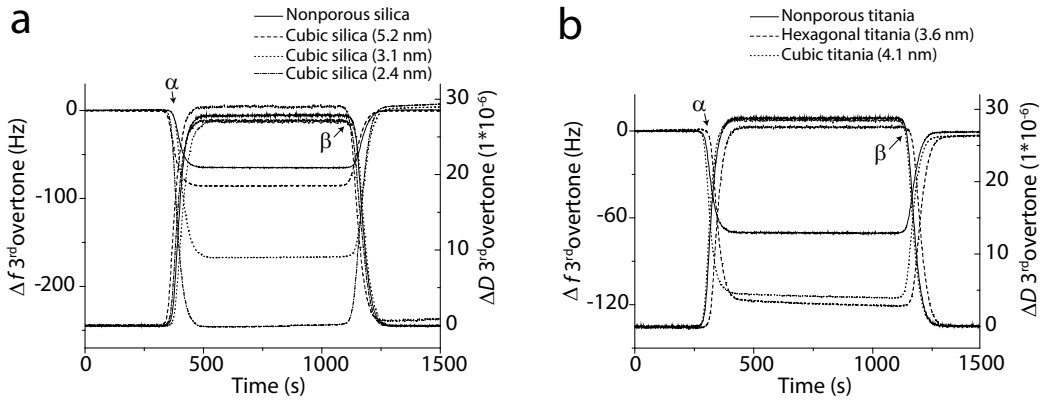


**Figure 21.** QCM-D results presenting the adsorption of water ($H_2O$) and deuterium oxide ($D_2O$) on mesoporous and nonporous (a) silica and (b) titania substrates. In the graphs, the shift in frequency (Δf) and dissipation (ΔD) against time are presented for (α) the replacement of $H_2O$ with $D_2O$ and (β) the replacement of $D_2O$ with $H_2O$.

Results showed that the pore volume was largest for cubic mesoporous silica having the smallest pores (2.4 nm) and decreased with increasing pore size. Mesoporous cubic and hexagonal titania had comparable pore volumes. The thickness of the thin films was observed in SEM to vary for the different mesoporous materials. In Table 1., results from SEM, QCM-D and nitrogen adsorption-desorption measurements the measured thicknesses, the areal mass/film thickness and specific surface area are presented.

**Table 1.** Measured film thickness, areal mass, areal mass/film thickness and specific surface area using SEM, QCM-D and nitrogen adsorption-desorption measurements, respectively. The areal mass/film thickness data are based on QCM-D results obtained by measuring the frequency difference between $H_2O$ and $D_2O$.

| **Mesoporous material (pore size)** | **Film thickness (nm)** | **Areal mass (μg/cm²)*** | **Areal mass/film thickness (g/cm³)*** | **Specific surface area (m²/g)**** |
|---|---|---|---|---|
| Nonporous silica (-) | 190 | 113 | 5.94 | - |
| Cubic silica (5.2 nm) | 350 | 150 | 4.29 | 249 |
| Cubic silica (3.1 nm) | 280 | 287 | 10.25 | 232 |
| Cubic silica (2.4 nm) | 210 | 431 | 20.52 | 733 |
| Nonporous titania (-) | 160 | 124 | 7.75 | - |
| Hexagonal titania (3.6 nm) | 180 | 203 | 11.28 | 125 |
| Cubic titania (4.1 nm) | 160 | 213 | 13.31 | 72 |

*The value of the areal mass corresponds to pure water.
**BET values

## 4.2 Meso-ordered hydrogels

The possibility of forming meso-ordered PEG-DA hydrogels templated with different triblock copolymers (L121 [$EO_5PO_{68}EO_5$], P123 [$EO_{20}PO_{70}EO_{20}$], L64 [$EO_{13}PO_{30}EO_{13}$] and F127 [$EO_{100}PO_{65}EO_{100}$]) was examined using SAXS and PLM. Also, the impact the length of the PEG-DA had on the formed materials was investigated (1.5K, 3.4K and 8.0K). As discussed in **Paper IV**, ordered hydrogels were only obtained when P123 was used as structure directing agent together with shorter PEG-DA segments (1.5K and 3.4K). In PLM, this order was observed to be anisotropic since birefringency was observed. In SAXS diffractograms Bragg peaks representing order were also seen. The other tested structure directing agents did not induce any order in the materials. The most hydrophobic amphiphile, L121 (HLB = 1), had a strong tendency to self-associate resulting in phase separation. As a consequence, no hydrogels could be made using L121. For the more hydrophilic amphiphiles (L64; HLB = 15 and F127; HLB = 22), the hydrophilic interaction between the long EO segments in the amphiphiles and the PEG-DA segments dominated in the systems, which gave unordered hydrogels. These results demonstrates that the hydrophilic-hydrophobic balance of the amphiphile determines the interaction with the PEG-DA segments and thereby the possibility of forming meso-ordered hydrogels. The HLB for P123 is 8, which seems to match well with the used PEG-DA to induce an ordered material [61]. Typical PLM results for precursor solutions and cross-linked hydrogels with and without template present prepared using P123 as structure directing agent, as well as a pure hydrogel is shown in Fig. 22.

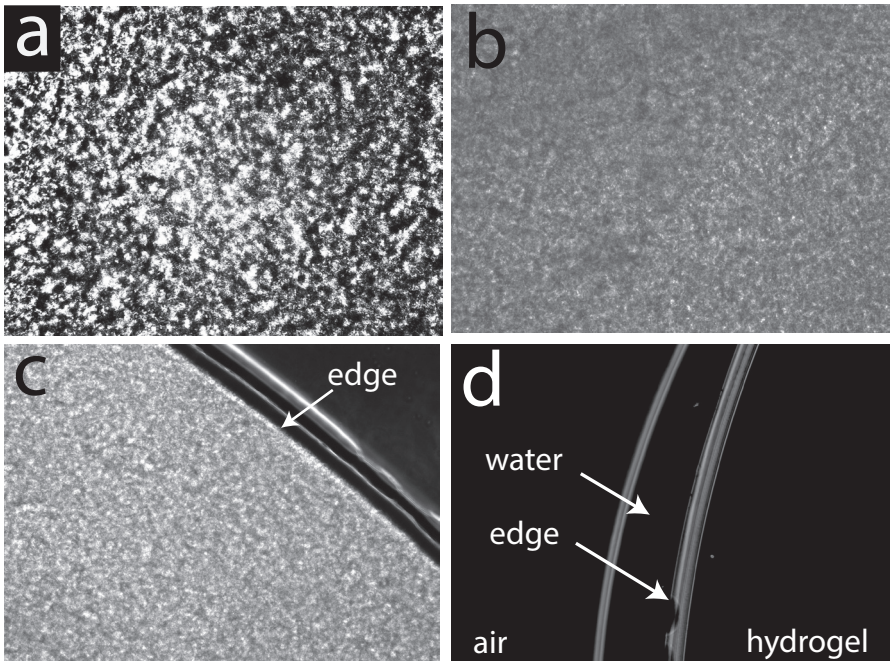


**Figure 22.** PLM micrographs of PEG-DA(1.5K)-50%(P123, 20%) (a) precursor solution, (b) cross-linked hydrogel with structure directing agent present, (c) hydrogel after removal of the structure directing agent, and in (d) PEG-DA(1.5K)-50%(P123, 0%) hydrogel. All hydrogels were fully swollen in water prior to analysis. In (c) and (d) the edge of the hydrogels are shown according to the arrows.

The water content of hydrogels prepared at different PEG-DA concentrations (20 wt%, 35 wt% and 50 wt%) and P123 concentrations (0-50 wt%) with and without structure directing agent present was calculated according to Eq 6.

$$\text{water content} = (W_s - W_d)/W_s * 100 \quad (6)$$

where $W_s$ and $W_d$ is the fully swollen and the vacuum dried weight of the hydrogels, respectively. The results from the swelling measurements, shown in Fig. 23., demonstrated that the water content increased with increasing amount of P123 and decreased with increasing concentration of PEG-DA, here noted as PEG-DA-20% for a sample containing 20% PEG-DA and 80% water etc. These trends reflect that the capacity of the water uptake can be adjusted by the concentration of PEG-DA and P123. No significant difference in water content was observed for hydrogels before or after removal of the structure directing agent.

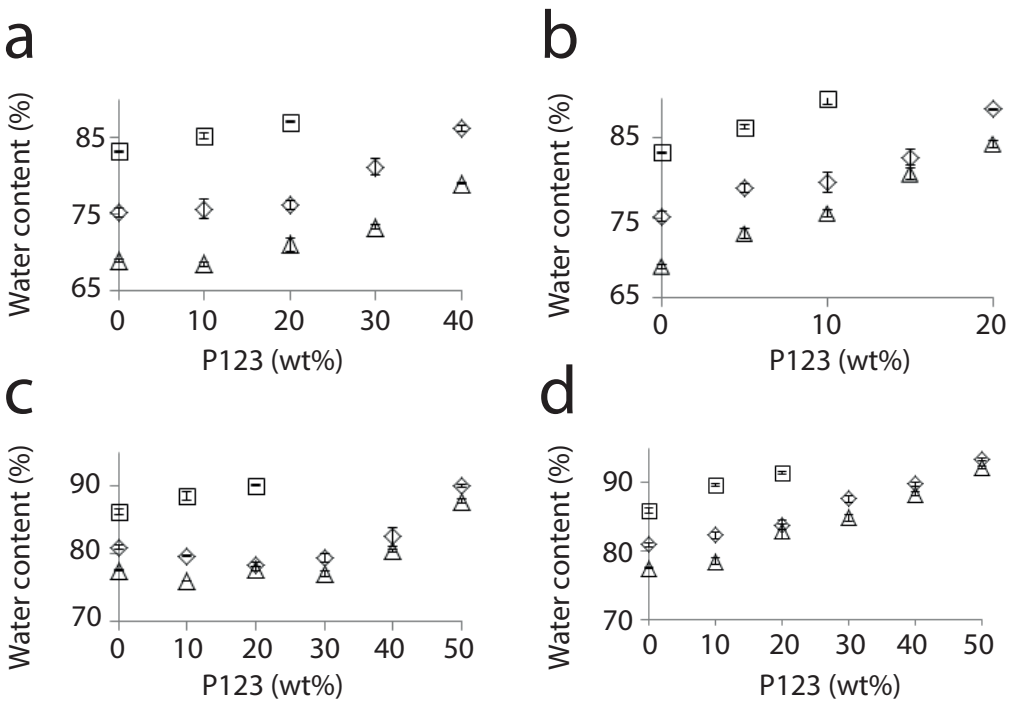


**Figure 23.** Water content measurements of PEG-DA hydrogels at varying precursor concentrations of PEG-DA (where □ = PEG-DA-20%, ◇= PEG-DA-35% and △= PEG-DA-50%) and P123 (0 to 50%). (a) and (c) show results obtained for PEG-DA(1.5K) and PEG-DA(3.4K) with the structure directing agent present, and (b) and (d) show results for PEG-DA(1.5K) and PEG-DA(3.4K) without the structure directing agent present. The error bars represent the deviation among three separate measurements.

SAXS measurements performed on precursor solutions and cross-linked PEG-DA hydrogels with and without structure directing agent present confirmed that precursor solutions and the hydrogels with structure directing agent present were ordered as is presented in Fig. 24. The peaks appeared at equal spacing in the SAXS diffractograms, which is typical for lamellar structures [89]. This lamellar structure was obtained for precursor solutions and hydrogels when the structure directing agent was still present, however, the peaks were more pronounced for hydrogels with higher PEG-DA concentrations. In the figure, arrows point out the origin of each peak, PEG or P123. The PEG peak corresponds to the distance between cross-link junctions [90].

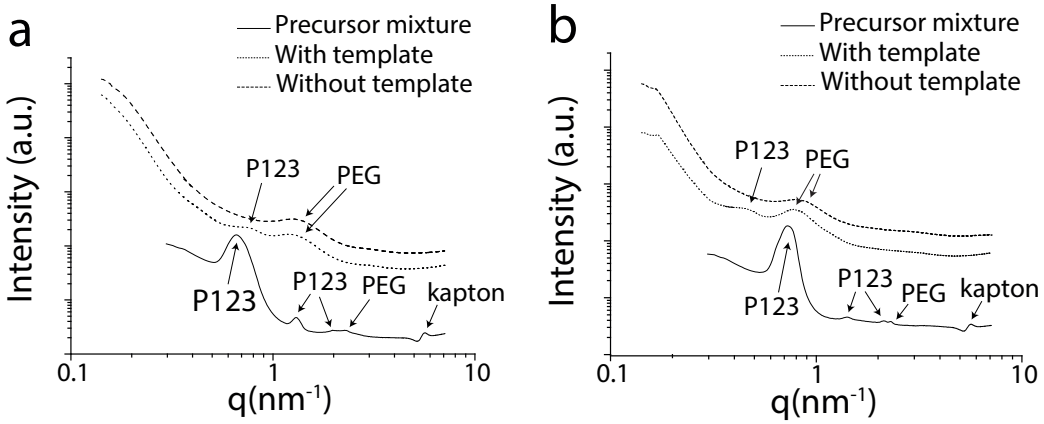


**Figure 24.** SAXS results presented as the arbitrary intensity (I) as a function of the q-value ($nm^{-1}$) of precursor solutions and hydrogels with and without structure directing agent present. (a) PEG-DA(1.5K)-50%(P123, 30%) and (b) PEG-DA(3.4K)-50%(P123, 30%).

Overall, more peaks were obtained in the precursor solutions than in the cross-linked hydrogels indicating higher order in the precursor solutions. The reason for this difference in number of peaks is hypothesized to be due to that PEG-DA segments became more restricted upon cross-linking resulting in less ordered structures. The P123 peak shifted to lower q-values with increasing concentration of PEG-DA, which implies that the distance between the lamellar sheets within the meso-ordered domains increased slightly with increasing P123 concentration.

Using SAXS, no lamellar order was observed for hydrogels after removal of the structure directing agent, which contradicts the observations made using PLM. Probably, a lamellar-like structure was present also in hydrogels after removal of the structure directing agent, however, this structure could not be confirmed via SAXS. The reason for this contradictory result is most likely due to that the water molecules, organized between the lamellar sheets after washing out the structure directing agents, do not scatter X-Ray light as strongly as the hydrophobic domains, such as cross-link junctions and the hydrophobic part of the P123 molecule. Hence, after removal of the P123, the contrast between the ordered domains is too weak to give rise to Bragg peaks.

Cross-linked hydrogels prepared without a structure directing agent were fully transparent, whereas hydrogels formed with P123 present contained small whitish opaque regions, which are suggested to be phase separated domains. These regions increased in size and amount with increasing concentration of P123. At high P123 concentration the whole hydrogel became opaque. It was also noticed that the hydrogels became weaker with increasing P123 concentration. These two observations in the physical appearance of the hydrogels together with the PLM and SAXS results suggested that the hydrogels contained lamellar domains at low P123 concentration and that the size and amount of these domains increased with increasing concentration of P123. Based on these speculations, the microstructure of the ordered hydrogels would look like the illustration shown in Fig. 25.

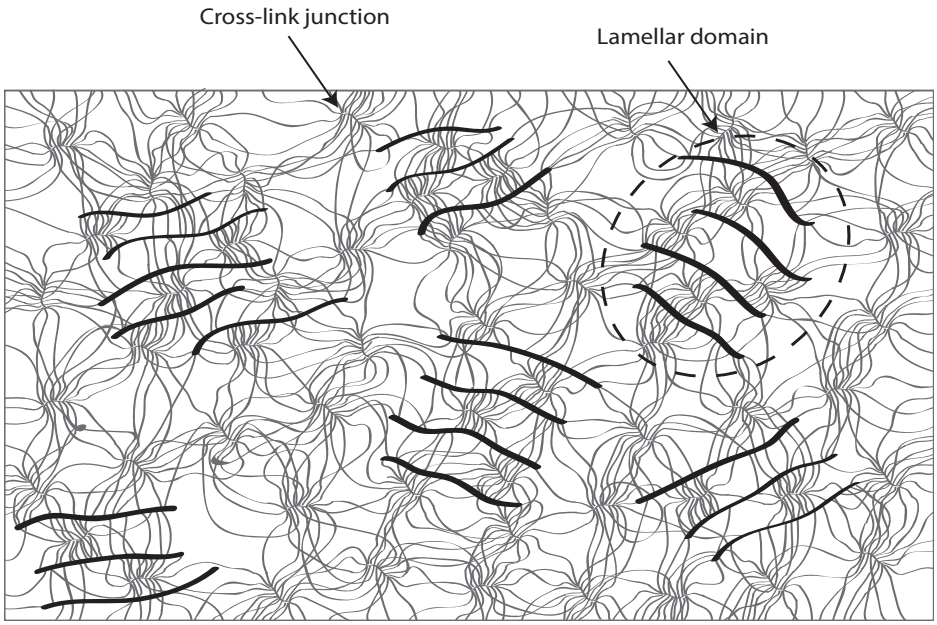


**Figure 25.** Illustration of the formed mesostructured hydrogel containing lamellar domains and cross-link junctions. The black lines in the lamellar domains correspond to the self-assembly of P123 molecules. The schematic is not drawn to scale.

The reason for only observing lamellar-like structure regardless of the concentration of P123 is likely due to that it is entropically unfavorable for these rather long PEG-DA segments to exist in other confined dimensions, such as cubic and hexagonal LLC systems [61]. Shorter PEG-DA molecules (0.258K and 0.575K) have, however, previously been shown to form other structures, such as hexagonal, by varying the amount of amphiphile [91-93].

The introduction of meso-order in hydrogels makes it possible to tune the properties of hydrogels, such as the water content and molecular transport, to match the demand for certain applications. This is interesting in e.g. tissue engineering applications.

## 4.3 PEG-based Hexosomes

Hydrogel particles were synthesized by covalently cross-linking PEG-DA using UV radiation in the presence of a water in oil (w/o) emulsion, were surfactants (Span80, HLBspan80 = 4.3 [66, 67]) were used both as structure directing agent and emulsifier. Results showed that particles were successfully formed when Span80 was used as structure directing agent whereas no bulk hydrogels could be prepared using the same surfactant. Probably, Span80 was to hydrophobic to interact with the hydrophilic PEG-DA segments when the synthesis was performed under hydrophilic conditions, as in the case of bulk hydrogels, resulting in phase separation. These observations agree with results discussed in Section 4.2 and in **Paper IV**. The formed particles were shown to have a high stability in water and were possible to dehydrate and re-disperse in water without the addition of dispersion agents. From here on focus will be on the characterization of the formed hydrogel particles as compare to pure bulk hydrogels.

Fully swollen particles and pure bulk hydrogels were examined by DLS, TEM, SAXS, PLM, and NMR. TEM analysis were performed on replicas of fully swollen particles prepared according to the mica sandwich technique or on embedded particles in agarose gel and on replicas of fully swollen bulk hydrogels prepared following the freeze etching technique. The particles were observed in TEM micrographs to be spherical and porous with a pore size of about 5 nm, Fig. 26. Cross-link junctions were observed as darker (elevations) and lighter (holes) regions on the sample surface for particles prepared following the mica sandwich technique and were shown to be randomly distributed with a distance of about 3 to 5 nm, see Fig. 26b. In DLS, the average size of the particles was measured to be 267 ± 21 nm.

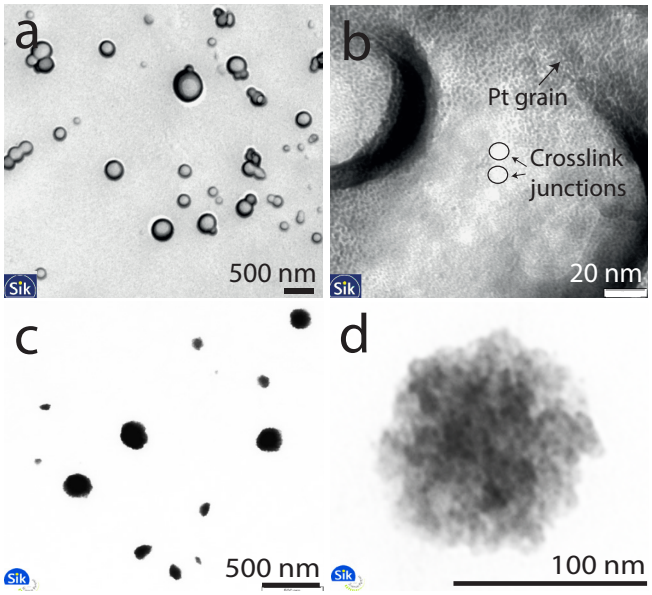


**Figure 26.** TEM micrographs demonstrated that the synthesized PEG-DA particles were spherical with varying sizes as is shown for particles prepared according to the mica sandwich technique in Fig. a-b and for embedded particles shown in Fig. c-d. The particles were observed to be porous with a pore size about 5 nm as is visualized in Fig. d. In Fig. b cross-link junctions and Pt grains (originating from the sample preparation) are highlighted.

Pure bulk hydrogels had a more open framework than the particles with pores spanning from a few nm to a few μm (see Fig. 27).

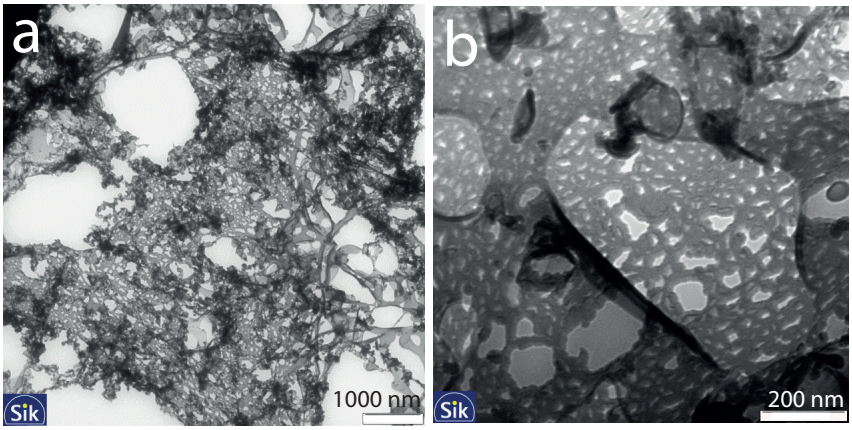


**Figure 27.** Bulk hydrogels without template present prepared according to the freeze etching technique.

SAXS measurements showed that the particles were ordered, which is seen as sharp peaks in the diffractogram (see Fig. 28). The position of the peaks for the hydrogel particles refers to a hexagonal order. Pure bulk hydrogels were as expected observed to be unordered. The peaks marked with a star (*) in both diffractograms represent the cross-link junction distance between PEG-DA segments in the samples [90, 94]. This peak was observed at higher q values for the particles than for pure bulk hydrogels demonstrating that the cross-link junction distance was shorter within the particles ($distance_{particle}$ = 3.7 nm, $distance_{bulk\ hydrogel}$ = 5.2 nm) even though the segment length of the PEG-DA molecule was the same for both samples. This result explains the different features of the hydrogels as was observed in TEM micrographs, with particles being denser. The molecular size of PEG-DA is known to determine the distance between cross-link junctions in hydrogels [90], which is contradictory to the obtained results. Most likely, the shorter cross-link junction distance observed in the particles was due to spatial restrictions of the hydrophilic PEG-DA segments during the formation of particles in the hydrophobic environment. These restrictions are also suggested to be responsible for the formation of hexagonal structured hydrogel particles where the emulsifier (Span80) is believed to self-assembly into hexagonal LLC's onto which PEG-DA segments are adsorbed and cross-linked.

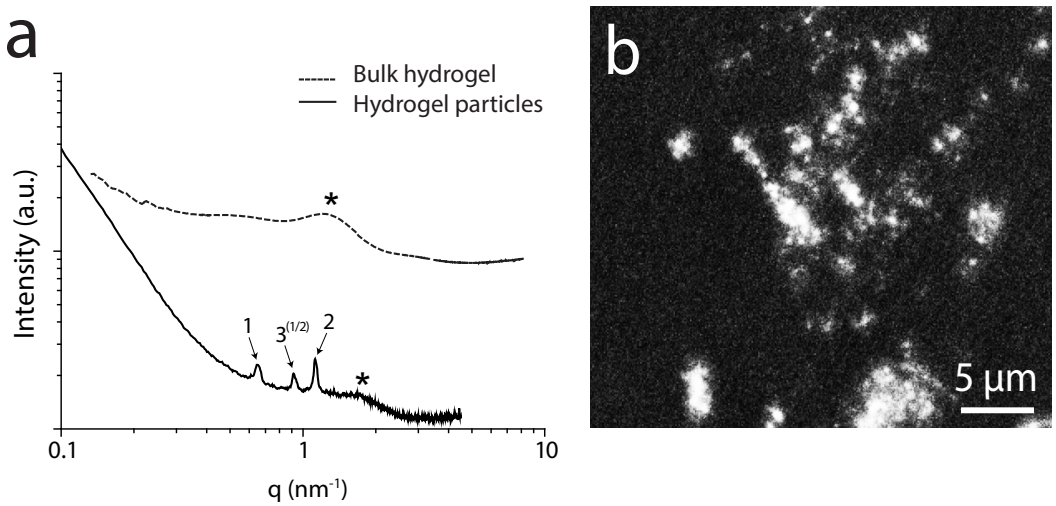


**Figure 28.** SAXS diffractograms in (a) showing the arbitrary intensity as a function of the q-value ($nm^{-1}$) for hydrogel particles (PEG-DA(1.5K)) and a pure bulk hydrogel (PEG-DA(1.5K)). The * indicate the peak responsible for the distance between cross-link junctions within the hydrogels and the arrows show Bragg peaks corresponding to a hexagonal structure within the hydrogel particles. In (b) PLM results demonstrated that the particles scattered polarized light, which confirmed the presence of long range order within the sample.

In PLM, polarized light was observed to be scattered by the hydrogel particles confirming the presence of anisotropically order, e.g. hexagonal or lamellar, see Fig. 28b. The exact order could not be obtained in the micrographs, however it is believed that the particles are hexagonally ordered because of the apparent SAXS results. From PLM it could also be concluded that the majority of the particles had a long-range order, showing that the synthesis procedure results in homogeneous samples.

The pore size and the volume fraction were calculated to be 4.6 nm and 0.76, respectively. These calculations were based on the estimated distance between the center of two pores in SAXS diffractograms and the size of Span80 as is further discussed in supplementary information in **Paper V**.

In **Paper IV** it was concluded that only lamellar structured bulk hydrogels could be formed when rather long PEG-DA segments were used, such as PEG-DA(1.5K). Here we demonstrate that PEG-DA(1.5K) also can form other structures than lamellar by performing the synthesis in a w/o emulsion. This result shows that the spatial restrictions in the system have an important influence on the formation of ordered hydrogels when using rather long PEG-DA segments.

Ordered hydrogel particles are of particular interest in drug delivery applications due to that these can provide a higher stability in the body than other suggested ordered delivery matrixes, i.e. cubosomes and hexosomes [95, 96]. A higher stability is advantageous in drug delivery applications since the life time of the device would be prolonged in the body and consequently results in a better and safer delivery of therapeutics. Also, the flexible hydrogel structure combined with well-ordered pores enables the loading of a large variety of therapeutics.

# Chapter 5

## Vesicle adsorption on silica, titania and PEG-DA

In this chapter, results on the formation of lipid bilayers via vesicle fusion on mesoporous silica and mesoporous titania as well as on pure PEG-DA bulk hydrogels are presented and discussed. Results on the formation of tethered lipid bilayers to mesoporous silica are also included.

### 5.1. Bilayer formation on mesoporous silica and titania

Lipid bilayers on solid supports are promising to use in the construction of biomimicry devices since their properties are similar to the living cell membrane. In order to use bilayers in such a device they should be continuous and homogenously spread on the support. It has previously been shown that vesicles adsorb differently on different types of surfaces depending on the composition of lipids in the vesicle (e.g. nonionic and/or ionic lipids), properties of the solution (pH, ion types and concentration) and the properties of the surface. The choice of lipids and surface has been demonstrated in previous studies to play a major role in the vesicle adsorption behavior, which is believed to be due to the electrostatic interactions between the surface and the vesicles [97-103]. Vesicles consisting of phospholipids have for example been observed to adsorb intact on titania [99, 104, 105] and gold [82] and to form lipid bilayers on silica [104, 105] and mica [106]. However, these characteristics have been shown to be possible to influence by adsorbing vesicles at different pH on silica and titania. Results have shown that vesicles (POPC or POPC with or without DGPP (1,2-di-(9Z-octadecnoyl)-sn-glycero-pyrophosphate)) adsorb intact on silica at high pH (pH ≥10) and that vesicles rupture and form lipid bilayers on titania at low pH (pH ≤ 2) [107, 108]. Furthermore, it has been shown that lipid bilayers can be formed on titania by increasing the ionic strength of the surrounding buffer [109, 110].

In the thesis, the focus was on comparing the adsorption of vesicles on mesoporous and nonporous silica and titania, **Paper I**, and on investigating the influence the pore size had on the formation of lipid bilayers on mesoporous silica, **Paper II**. The adsorption behavior of vesicles on the different surfaces was studied using QCM-D, FRAP and AFM. QCM-D results showed that lipid bilayers were formed on silica and that vesicles adsorbed intact on titania regardless of porosity, as is seen in Fig. 29. This is explained by differences in the electrostatic interactions between the surfaces and the vesicles. Silica has a lower isoelectrical

point (IEP ≈ 2 [111]) than titania (IEP ≈ 4-5 [111]), which implies that silica surfaces are more negatively charged at neutral pH. As a consequence, vesicles experience larger stress/strain forces on silica than on titania, which results in that vesicles are more prone to rupture and to form lipid bilayers on silica.

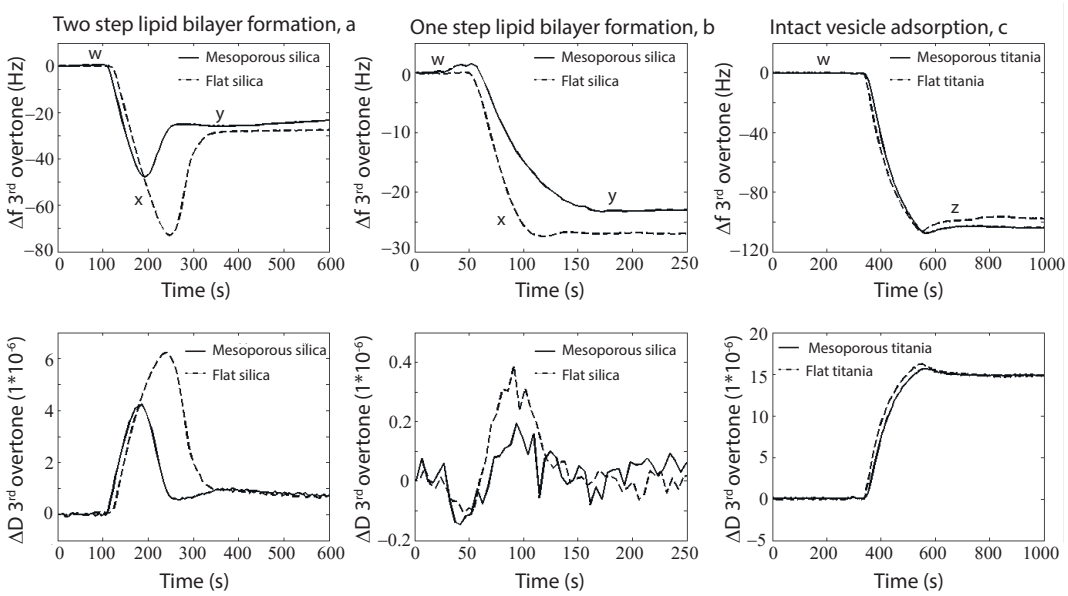


**Figure 29.** QCM-D results presented as shifts in frequency (Δf) and dissipation (ΔD) against time. The results showed that lipid bilayers were formed on mesoporous and nonporous silica (a) and (b) and that intact vesicles were adsorbed on mesoporous and nonporous titania (c). Lipid bilayers were formed more rapidly on mesoporous silica than on nonporous silica according to (a) and (b). In (a) vesicles were prepared and dispersed in PBS buffer before injection in the QCM-D instrument, which resulted to a two-step formation of bilayers and in (b) vesicles were prepared in pure water and dispersed in PBS buffer before injection in the QCM-D resulting in a one-step formation of bilayers. Vesicle injection, w, vesicle rupture, x, lipid bilayer formation, y, and intact vesicles adsorption, z are indicated in the figures.

Lipid bilayers were observed to form via a one-step process (direct rupturing of vesicles and formation of lipid bilayer upon adsorption on a surface) on both mesoporous and nonporous silica using vesicles prepared in pure water and dispersed in PBS just before injection in the QCM-D instrument, see Fig. 29b, and via a two-step process (intact vesicles are first adsorbed on a surface until critical concentration of vesicles is reached, at this point vesicles starts to rupture and from lipid bilayers) when vesicles were prepared and dispersed in PBS before injection, see Fig. 29a. This difference in adsorption behavior is suggested to be due to the osmotic pressure that is caused by the difference in ion concentration when no ions are present during the vesicle preparation (Fig. 29b). Water molecules from the inside of the vesicles are believed to diffuse through the lipid bilayer in order to establish equilibrium concentration of ions in the system. As a result, vesicles are exposed to a pressure from the inside causing a more rapid formation of lipid bilayers upon adsorption on a surface. QCM-D results also showed a difference in kinetics for the formation of lipid bilayers, with a more rapid formation of bilayers on mesoporous silica than on nonporous silica. This

was observed as a smaller shift in $\Delta f_{max}$ and $\Delta D_{max}$, which was interpreted as fewer vesicles needed in order to initiate bilayer formation. The pore size of mesoporous silica was furthermore shown to have an impact on the bilayer formation, with a more rapid formation of lipid bilayers on the surface having smaller pores. This conclusion was based on QCM-D measurements performed on mesoporous and nonporous silica having pore sizes of 6 nm, 4 nm and 2 nm, see Fig. 30.

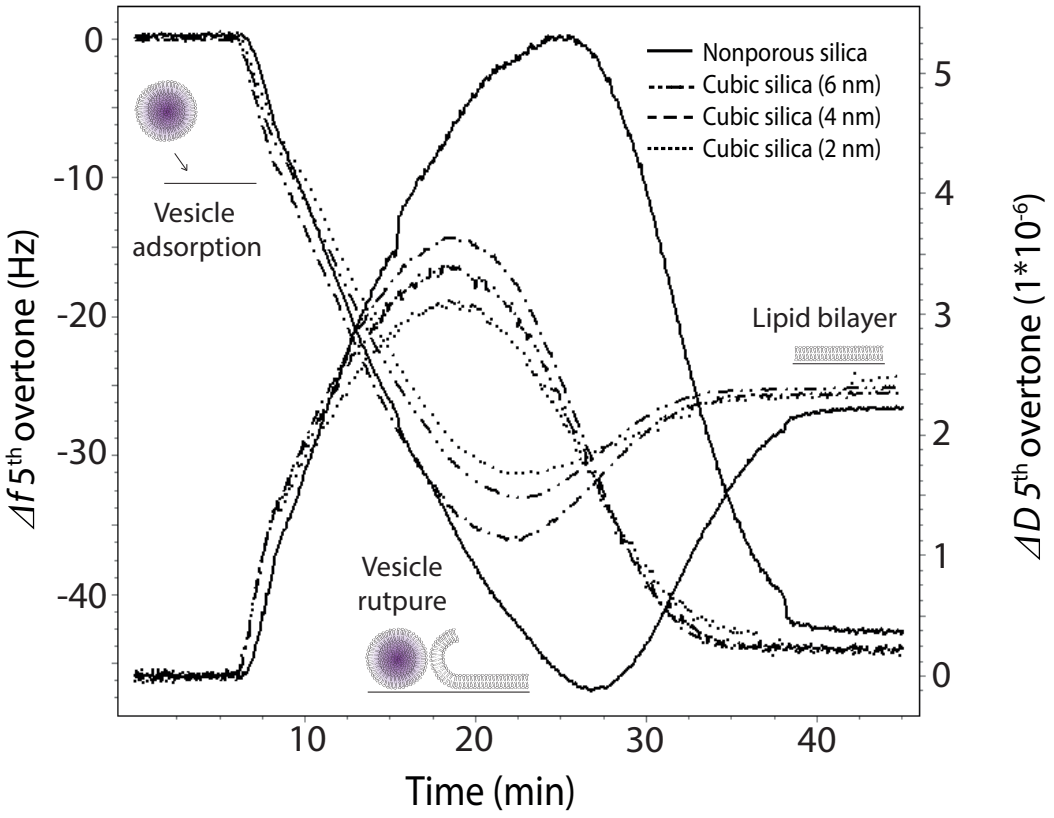


**Figure 30.** QCM-D results presented as shifts in frequency (Δf) and dissipation (ΔD) against time. According to the figure, lipid bilayers were formed on all surfaces with the most rapid formation of bilayers on the surface having the smallest pores (2 nm) and slowest on the nonporous surface. Schematics in the figure illustrates the adsorption of vesicles, followed by rupturing of vesicles at a critical concentration and finally formation of lipid bilayers.

The initial slopes in Δf and ΔD were similar on all surfaces regardless of porosity, which indicated that vesicles adsorbed similarly on all surfaces [74]. AFM studies on mesoporous (having a pore size of 6 nm) and nonporous silica confirmed these results by comparing height and diameter of the adsorbed vesicles (see **Paper II**). According to AFM images shown in Fig. 31, bilayer patches from single vesicles were observed to be present to a larger extent on mesoporous silica than on nonporous silica, which is interpreted as that the interaction between the surface and the vesicles is favored when pores are present. These measurements were possible to perform by interrupting the adsorption process before the critical concentration of vesicles was reached on the two surfaces to avoid rupturing and formation of lipid bilayers.

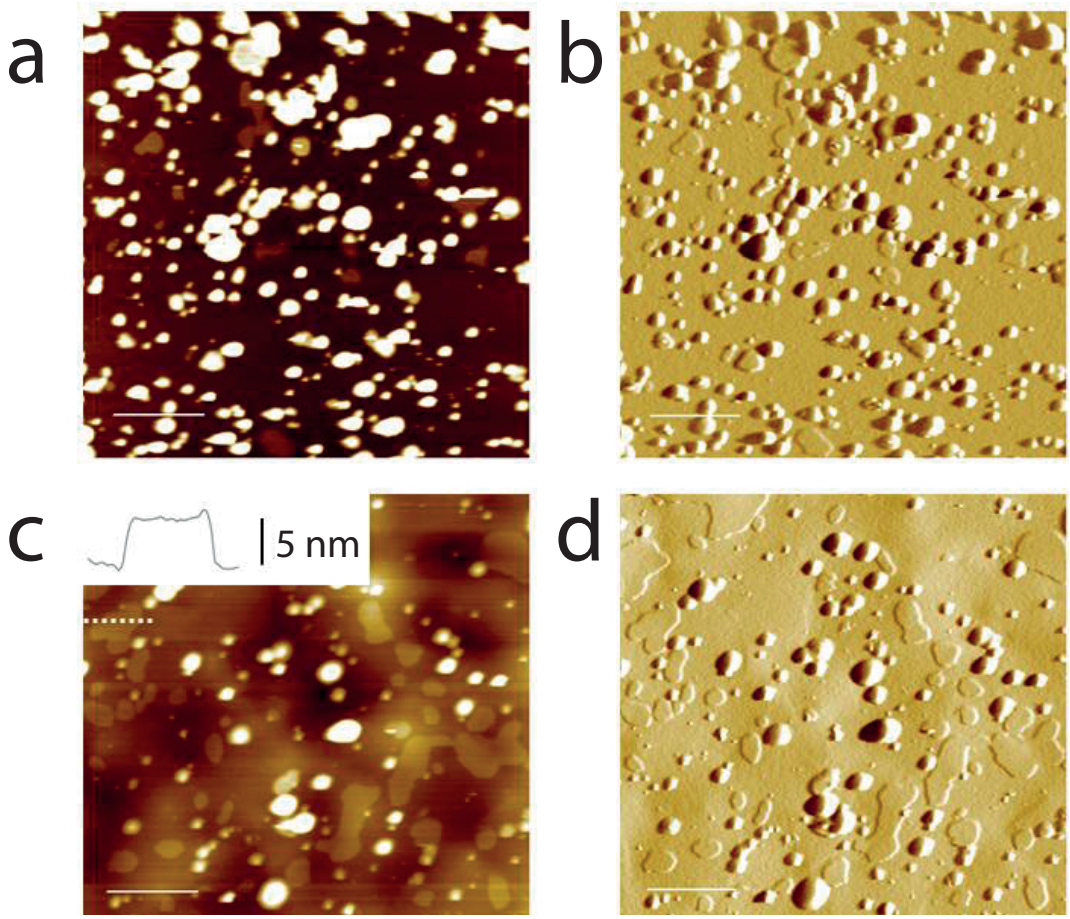


**Figure 31.** AFM images showing vesicles adsorbed on nonporous (a)-(b) and mesoporous silica (pore size 6 nm) (c)-(d). The surface topography is shown in image (a) and (c) and the corresponding deflection of the cantilever is shown in image (b) and (d). A cross section of a bilayer patch is presented as an inset in image c. Scale bar equals 1 μm

The presence of lipid bilayers was confirmed from AFM and FRAP analysis. These results concluded that the lipid bilayers were continuously spread and that they were fluidic on all the investigated surfaces. The lateral diffusion coefficient (D) was observed to differ on the various surfaces with the slowest diffusion of lipids on mesoporous silica having the smallest pore size. The diffusion rate increased with increasing pore size and was observed to be largest on the nonporous surface according to Table 2.

**Table 2.** FRAP results showing the calculated lateral diffusion coefficients (D) and immobile fraction ($\gamma_0$), defined as immobile molecules in the bilayer, on nonporous silica and mesoporous silica having a pore size of 2, 4 and 6 nm [31].

| **Pore size (nm)** | **Diffusion coefficient (D) ($\mu m^2/s$) (n = 6)** | **Immobile fraction ($\gamma_0$) (%)** |
|---|---|---|
| nonporous | 2.78 ± 0.06 | 0.5 |
| 6 | 2.01 ± 0.04 | 1 |
| 4 | 1.89 ± 0.01 | 1 |
| 2 | 1.80 ± 0.03 | 4 |

The difference in diffusion coefficients was suggested to be due to the difference in hydrophilicity of the surfaces, which is known from previous studies to have a large impact on the bilayers. This correlated well with the measured surface tensions ($\gamma_c$), which was shown to be highest on the surface having the smallest pores and lowest on the nonporous surface, as discussed in **Paper II**.

To summarize the results from the bilayer studies on the examined silica and titania surfaces, the nature of the surface was observed to determine the adsorption behavior of vesicles. On titania, vesicles adsorbed intact and on silica lipid bilayers were formed regardless of porosity. Lipid bilayers were observed to form more rapidly on mesoporous silica than on nonporous silica with the most rapid formation on the surface having the smallest pores (2 nm).

For the construction of biomimetic devices based on supported lipid bilayers, mesoporous silica having a pore size similar to the thickness of lipid bilayers (~5 nm) is considered to be promising to use as support material. However, the stability of bilayers on such supports is still unknown and needs to be further investigated.

## 5.2. Vesicle adsorption on PEG-DA hydrogels

The adsorption of vesicles was evaluated on a soft support (PEG-DA(1.5K)) using QCM-D and FRAP. The strategy was to couple PEG-DA molecules to modified (3(acryloyloxy)propyl trimethoxysiliane, APTMS) mesoporous silica using spin coating (2000-4000 rpm) or freely adsorb PEG-DA onto the surfaces followed by cross-linking via UV radiation, see Fig. 32. FRAP measurements were only performed on non-covalently attached free-standing hydrogels.

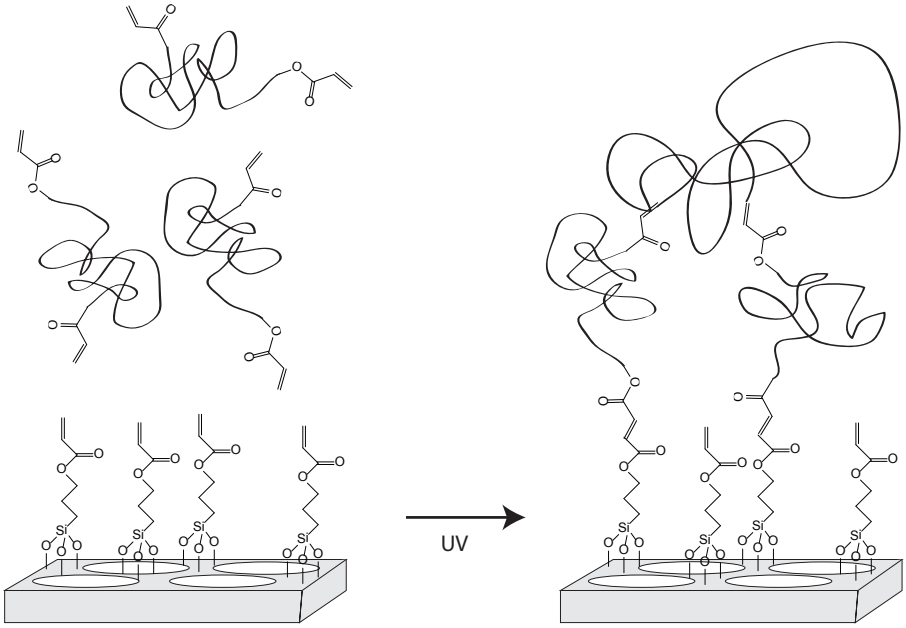


**Figure 32.** Illustration of PEG-DA molecules that covalently bind to an APTMS modified mesoporous silica surface followed by cross-linking to form a covalently attached hydrogel.

QCM-D results showed that the coupling between PEG-DA molecules and the modified surface was incomplete regardless if the PEG-DA molecules were spin coated (Fig. 33a) or let to adsorb freely from solution (Fig. 33b) onto the surfaces. This conclusion was based on QCM-D results since an increase in frequency and a decrease in dissipation upon rinsing with water were observed. POPC vesicles were shown to adsorb onto the hydrogels. In Fig. 33a a bilayer seems to be formed via a two-step process, but parts of the bilayer is desorbed upon rinsing, which is observed as an increased frequency. The continuing decrease in dissipation showed that the adsorbed film became more rigid with time, which is suggested to be due to that PEG-DA molecules desorbed from the surface. In Fig. 33b the frequency decreased to about -26 Hz upon addition of vesicles while the dissipations remained similar indicating that a bilayer was formed via one-step process onto the PEG-DA hydrogel.

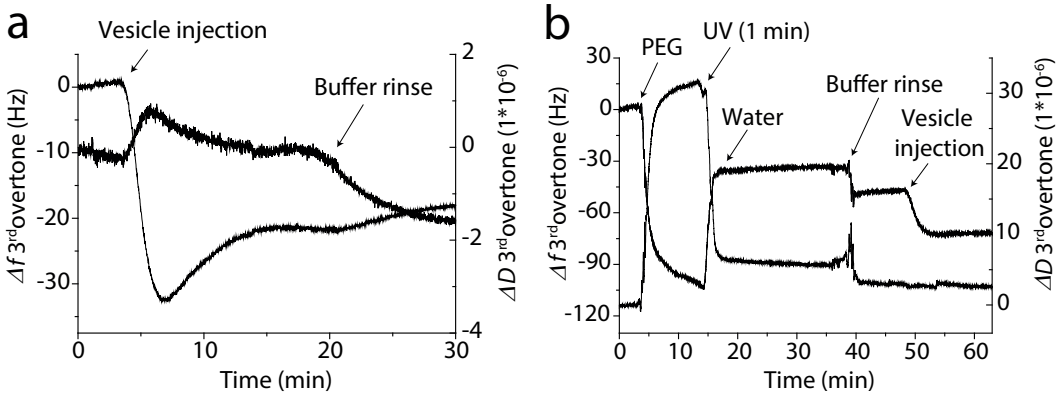


**Figure 33.** Vesicle (POPC) adsorption on PEG-DA(1.5K). In (a) PEG-DA was spin coated and cross-linked on modified silica crystals at a spin rate of 3000 rpm prior to analysis and in (b) PEG-DA was cross-linked in situ in QCM-D flow cell via UV light. In the figure, a PEG-DA(1.5K) concentration of 10 wt% and 5 wt% were used in (a) and (b), respectively.

Using FRAP, lipids were observed throughout the hydrogel (PEG-DA(1.5K)-20%), according to Fig. 34. Since hydrogels were shown to have an open structure with pores ranging from a few nm to a few μm according to TEM micrographs (section 4.3 and **Paper V**) it is reasonable that vesicles might penetrate the hydrogel. The large white spots in the figure are larger than the size of a vesicle indicating that bilayer patches were present within the hydrogel.

**Figure 34.** Typical FRAP measurement showing vesicle absorption on PEG-DA(1.5K)-20%.

## 5.3. Tethered lipid bilayers on mesoporous silica

It is possible to covalently anchor lipid bilayers to different surfaces using "spacers" with functional end groups, so called tethers. The purpose of the tether is to increase the stability of the lipid bilayer and simultaneously create an increased space between the bilayer and the support, as is illustrated in Fig. 35.

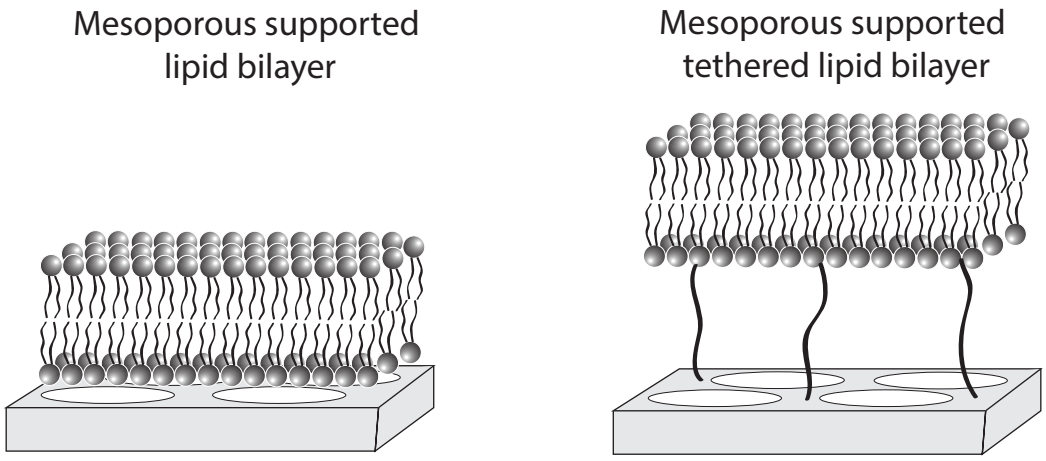


**Figure 35.** A schematic illustrating (a) a supported lipid bilayer and (b) a tethered lipid bilayer on a mesoporous surface.

One example of a "spacer" between lipid bilayers and supports are polymer cushions, which are shown to serve as a lubricant for the bilayer and also to decrease nonspecific binding of macromolecules to the surface [112]. Moreover, polyethylene glycol (PEG) having different chain lengths have been used to covalently anchor a lipid bilayer to a surface [48, 113, 114].

The aim with this part of the thesis was to covalently anchor lipid bilayers to amine modified mesoporous and nonporous silica using PEG molecules as tethers. Tethered lipid bilayers (TLBs) were proposed to form via vesicle fusion by adsorbing POPC vesicles containing 2 mol% tethers (DSPE-PEG2000-NHS) with respect to POPC lipids on the surfaces. The advantage of forming TLBs in such a manner is that a lower amount of tethers is needed compare when first anchoring tethers to a surface followed by vesicle fusion on top of the tethered surface [48]. QCM-D measurements were performed to monitor the bilayer formation and AFM was used to verify the presence of TLBs on the surfaces. Also the thickness of the bilayer and the mobility of the lipids in the TLBs were investigated via square tests using AFM. In the study cubic mesoporous silica thin films having a pore size of 6 nm was used.

QCM-D results demonstrated that tether containing vesicles adsorbed intact on the amine modified surfaces, according to Fig. 36. The vesicles did not show any tendency to rupture even when osmotic pressure or shear forces were applied. This ability for the vesicles to remain intact was attributed to weak surface-vesicle and vesicle-vesicle interactions. These interactions were weak because of strong

repulsion forces between the positive ions on the surface and the zwitterionic POPC lipids in the bilayer and the steric repulsion between the vesicles caused by the tethers sticking out from the vesicle surface. Moreover, the number of tether containing vesicles on the surface is probably less compare to pure lipid vesicles due to immediate covalent bonding between the tethers and the surface, hindering efficient packing. The vesicles were only observed to rupture and to form TLBs when amphipathic α-helical (AH) peptides were injected.

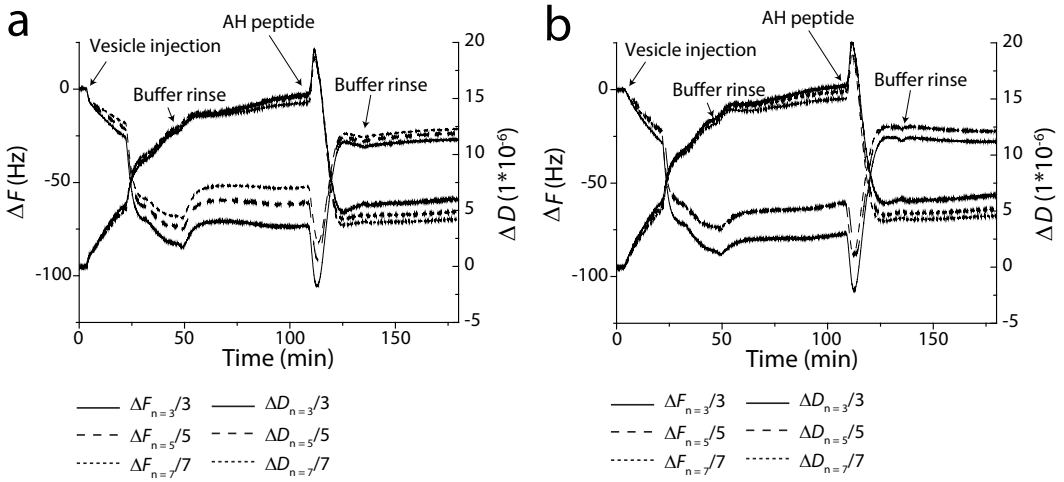


**Figure 36.** QCM-D results presented as shifts in frequency (Δf) and dissipation (ΔD) for the formation of TLBs on (a) nonporous and (b) mesoporous silica as a function of time. Intact vesicles on the surfaces ruptured forming bilayers upon injection of AH peptides.

The final frequency and dissipation shifts were -23 ± 2.9 Hz and 5.2 ± 0.8·$10^{-6}$, respectively on nonporous silica and -25 ± 3.0 Hz and 5.0 ± 0.9·$10^{-6}$, respectively on mesoporous silica. These shift are significantly different than those obtained in a previous study where non-covalently anchored lipid bilayers were formed using POPC vesicles containing 2 mol% $PEG_{2000}$-PE with respect to POPC lipids on nonporous silica surfaces. For these non-covalently attached bilayers the final frequency and dissipation shifts were - 37 ± 2.4 Hz and 2.2 ± 0.3·$10^{-6}$, respectively [115]. These differences are most probably due to the strong repulsion forces between the positively charged surfaces and the covalently anchored lipid bilayers resulting in more flexible bilayers. Flexible bilayers are observed in QCM-D as larger dissipation shifts. The reason for observing lower frequency shifts for the covalently attached bilayers is explained by bilayer thinning occurring upon adsorption of AH peptides, where the peptides are suggested to replace the lipids in the lower leaflet of the bilayer [116].

The presence of homogeneously spread TLBs on the surfaces was verified using AFM analysis, see Fig. 37. AFM images were taken directly after the TLB formation observed in QCM-D using the same crystals by transferring these in the wet state to the AFM instrument. Square test on the surfaces showed that the TLBs had a thickness of about 3-4 nm on nonporous silica and about 6-7 nm on mesoporous silica.

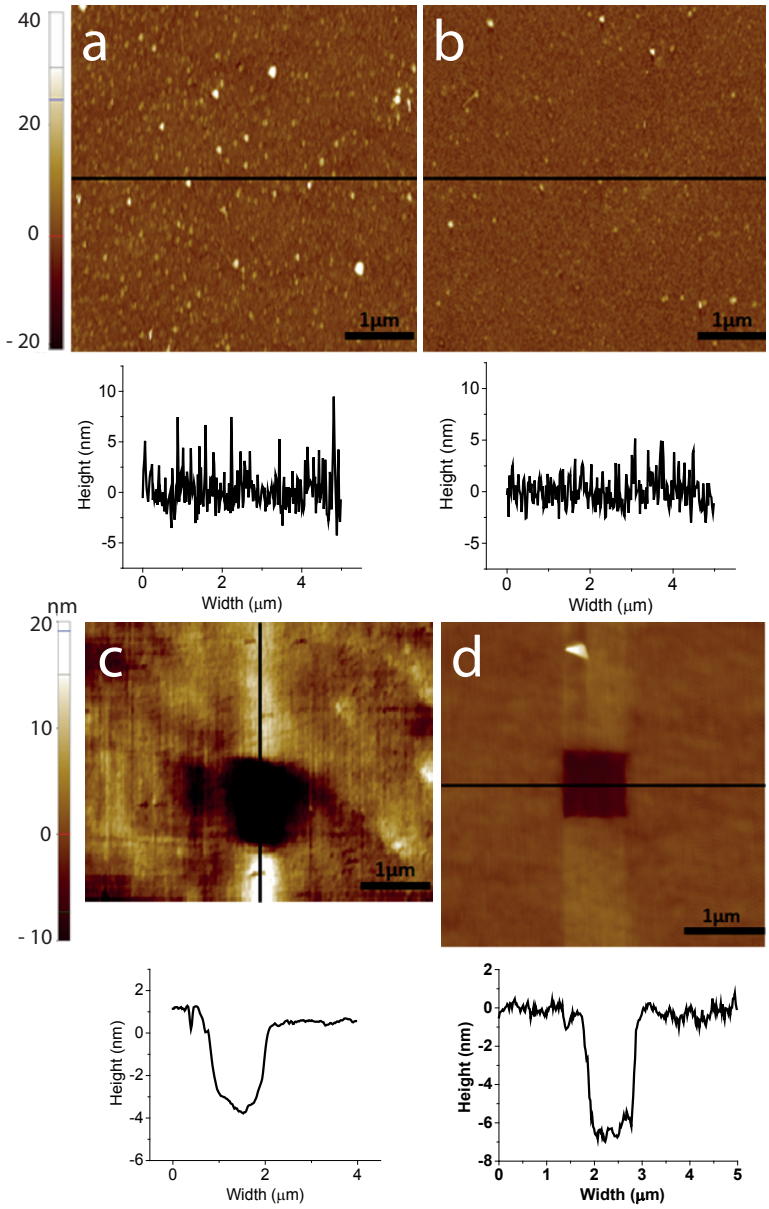


**Figure 37.** AFM images and square tests of TLBs on nonporous (a) and (c) and mesoporous (b) and (d) silica.

This difference in thickness is explained by the porosity of cubic mesoporous silica resulting in 42% smaller surface area available for tethers to bind to when assuming that tethers only bind to the wall between the pores. PEG molecules that are forced together upon adsorption to a surface has a stronger tendency to stretch out in solution, and as a consequence pushing the bilayer away from the surface (see Fig. 38), resulting in a thicker TLB [115]. Images taken 1h and 2h after square tests did not show any recovery of the squares indicating that the lipids in the TLBs were immobile at a micrometer range. AH peptides have previously been shown to impair the mobility of lipids in supported lipid bilayers, which explains the obtained results [116].

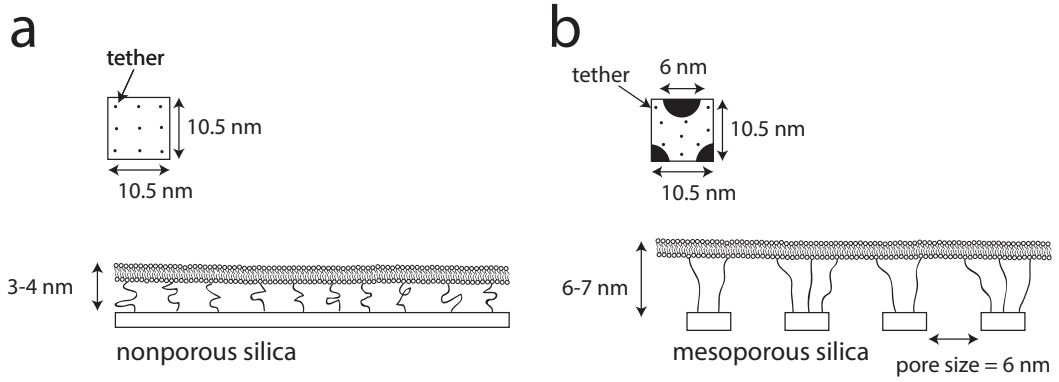


**Figure 38.** Schematic illustrates TLBs on nonporous silica (a) and on mesoporous silica (b).

To conclude, TLBs were successfully formed on amine modified mesoporous and nonporous silica surfaces via rupturing of tether containing vesicles using AH peptides, as illustrated in Fig. 39. From square tests performed using AFM, lipids in the TLBs were observed to be immobile. In the design of drug delivery vehicles, immobile lipids are not considered to have a large impact on the delivery process since drugs are suggested to be released upon degradation of the bilayer and not via free diffusion through the bilayer.

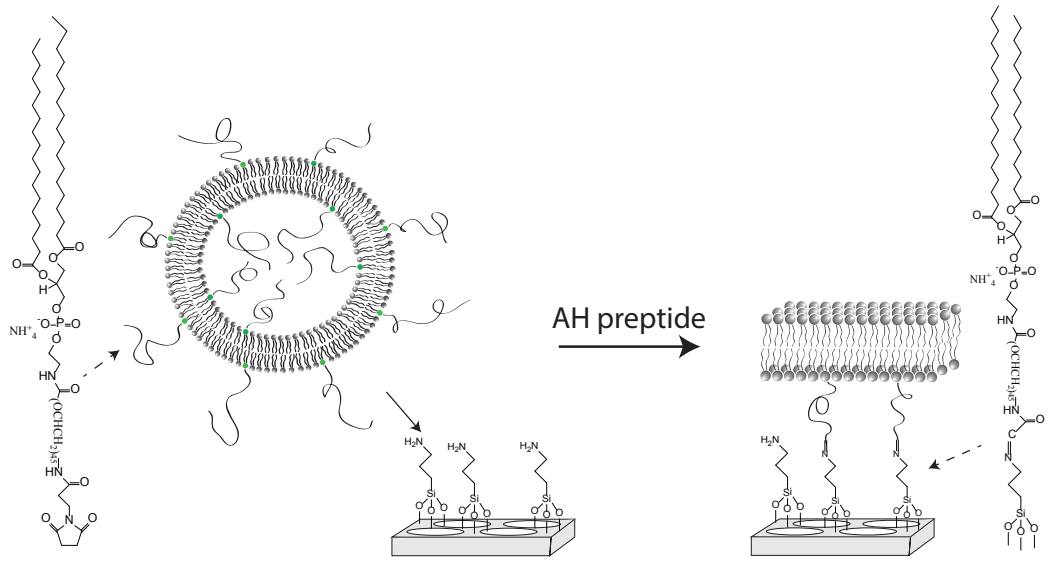


**Figure 39.** Schematic illustration on the formation of TLBs on an amine modified cubic mesoporous silica surface using AH peptide.

# Chapter 6

## Enhanced signal-to-noise ratio of the QCM-D signal

The detection of small analytes at low concentration is crucial in many biological and environmental applications [117]. One suggestion to improve the detection of such molecules is to increase the sensitivity of the QCM-D signal by using mesoporous materials as detecting surface [50]. The advantages of using mesoporous surfaces are that these provide a large surface area as compared to its nonporous counterpart and that their properties, such as pore size, pore geometry and surface chemistry, can be tailor made by the choice and amount of structure directing agent, the chemical composition and additional surface treatments [16, 63]. In this thesis the adsorption of different generations (GO, G1, G2 and G3) of PAMAM dendrimers on cubic mesoporous silica having varying pore size and on hexagonal and cubic hexagonal titania having similar pore size was investigated and discussed in **Paper III**. In Fig. 40, the size of the tested dendrimers together with the pore sizes and pore geometries of the used mesoporous materials are illustrated.

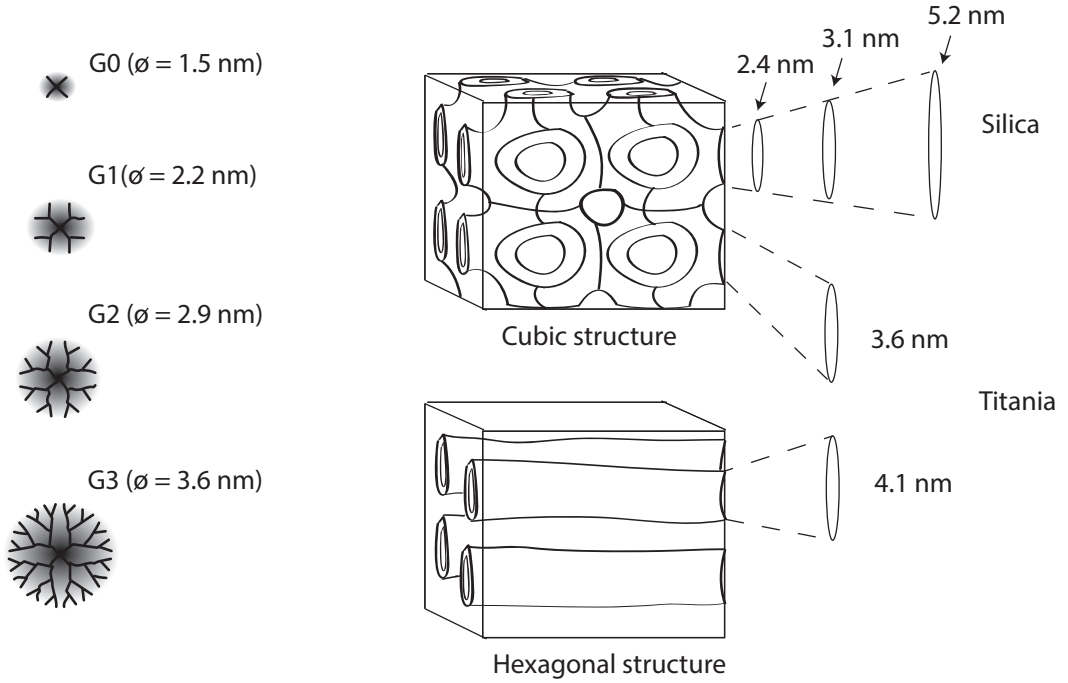


**Figure 40.** The schematic illustrates the size of the different generations (G0, G1, G2 and G3) of PAMAM dendrimers as well as the pore sizes and pore geometries of the used mesoporous materials.

The dendrimers were used to link their size to the pore size of the mesoporous materials. The properties of the tested dendrimers are presented in Table 3. Mesoporous and nonporous coated QCM-D crystal were prepared and compared.

**Table 3.** Information about the investigated PAMAM dendrimers; molecular weight, the number of surface groups ($NH_2$-groups), and diameter according to specifications and measured using DLS.

| Generation | Molecular weight (g/mol) | Surface groups | Diameter (nm) according to spec.*[118] | Diameter (nm) DLS (n = 3)* |
|---|---|---|---|---|
| G0 | 517 | 4 | 1.5 | 1.2 |
| G1 | 1 430 | 8 | 2.2 | 1.8 |
| G2 | 3 256 | 16 | 2.9 | 2.8 |
| G3 | 6 909 | 32 | 3.6 | 3.1 |

*PAMAM dendrimers dispersed in methanol.

The analytes having a smaller size than the pores can diffuse into the material, analytes that have comparable size as the pores of the material has limited access to the interior of the material whereas analytes having larger size than the pores are only interacting with the top surface of the mesoporous material.

Overall, the two smallest dendrimers were observed to get access to all the tested mesoporous materials resulting in an increased signal-to-noise ratio of the QCM-D is shown Fig. 41a for G1 dendrimers. It was furthermore shown that the largest pores (5.2 nm) were accessible for all tested dendrimers.

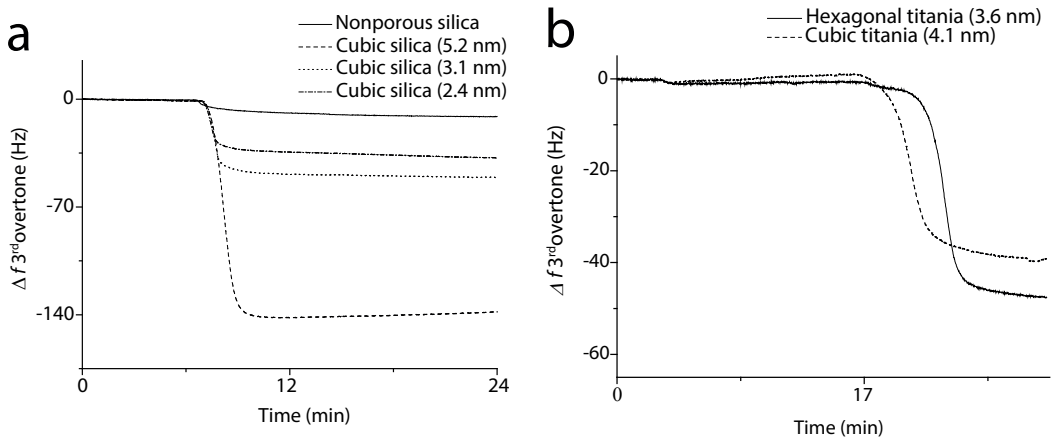


**Figure 41.** QCM-D results presented as a shift in frequency ($\Delta f$), showing the adsorption of G1 dendrimers on (a) cubic mesoporous silica having varying pore size and on (b) cubic and hexagonal titania having comparable pore size.

The shift in dissipation was small on all tested surfaces, which implies that the dendrimers either formed a solid like layer on the surface or diffused into the pores. This made it possible to study the improvement of the QCM-D signal by comparing the obtained Δf results of each surface with respect to the thickness of respectively film. A summary of the QCM-D results for dendrimer adsorption on mesoporous silica is presented in Table 4.

**Table 4.** Data representing the improved QCM-D signal-to-noise ratio that was obtained upon the adsorption of different generations (G0, G1, G2 and G3) of PAMAM dendrimers on cubic mesoporous silica having varying pore size compared with the nonporous counterpart.

| Dendrimer (ø) | Nonporous silica | Mesoporous silica (ø = 5.2 nm) | Mesoporous silica (ø = 3.1 nm) | Mesoporous silica (ø = 2.4 nm) |
|---|---|---|---|---|
| G0 (1.5 nm) | 1.0 | 38.5 | 38.5 | 83.6 |
| G1 (2.2 nm) | 1.0 | 12.3 | 4.5 | 3.4 |
| G2 (2.9 nm) | 1.0 | 16.9* | 2.2 | 1.9 |
| G3 (3.6 nm) | 1.0 | 14.4* | 3.5 | 1.5 |

*The final value was not reached.

Slightly higher amount of dendrimers was observed to adsorb on hexagonal titania than on cubic titania regardless of the size of the dendrimer, however the adsorption was shown to be more rapid on cubic titania as is presented in Fig. 41b for the adsorption of G1 dendrimers. The difference in adsorption is explained by the differences in surface area, which was shown in nitrogen adsorption-desorption analysis to be larger for the hexagonal than for the cubic material. It is likely that the adsorption was more rapid on cubic titania thin films because it has accessible pores on the upper surface as compare to the hexagonal thin films, which only has pores running parallel to the surface. This difference in pore arrangement implies that the diffusion of analytes into the pores is less hindered on cubic surfaces. The shift in frequency increased with increasing size of dendrimers from -25 Hz for G0 dendrimers to -70 Hz for G3 dendrimers. No dendrimers adsorbed on nonporous titania. This result demonstrates that analytes that have a low affinity for a certain material can be detected by introducing pores in the material, which implies that the observed frequency shift are due to differences in density.

By comparing the results obtained on cubic mesoporous silica and titania prepared using the same structure directing agent (P123, silica and titania with a pore size of 5.2 nm and 4.1 nm, respectively) a higher adsorption of dendrimers was observed on the silica surface regardless of the size of the dendrimer. This result along with the lack of adsorption on nonporous titania implies that the affinity between the dendrimers and the surface was higher on silica. This is reasonable since silica has a lower isoelectrical point (IEP ~ 2 [111]) than titania (IEP ~ 4-5 [111]), which results in that silica is more highly charged at neutral pH as is applicable in this study. Consequently, the PAMAM dendrimers are suggested

to bind to the walls of the mesoporous silica material and to float around in the pores of the mesoporous titania material resulting in a stronger signal on mesoporous silica.

To summarize, the sensitivity was demonstrated to be improved using mesoporous material as sensing surface. Based on these results, mesoporous materials are suggested to improve the signal-to-noise ratio of the QCM-D frequency signal, which may increase the probability to detect small concentrations of small analytes. Moreover, the analytes might be detected even though they are not adsorbed to the surface.

# Chapter 7

## Concluding remarks and outlook

The results presented in this thesis showed that mesoporous silica, titania and PEG-DA hydrogels can be formed using different types of structure directing agents, such as triblock copolymers and surfactants. In the formation of meso-ordered hydrogels, the synthesis conditions were demonstrated to have major impact on the pore orientation and morphology of the final material when rather long polymer segments were used as precursors. Mesoporous silica and titania were furthermore evaluated as a platform for covalently and non-covalently anchored lipid bilayers as well as the use of these as sensing surface to increase the sensibility of the QCM-D technique. The formation of lipid bilayers was also investigated on pure PEG-DA bulk hydrogels.

Vesicles were shown to rupture and form lipid bilayers on mesoporous and nonporous silica and to adsorb intact on titania regardless of porosity. The kinetics of the bilayer formation was observed to differ on mesoporous and nonporous silica with a more rapid formation on mesoporous silica. No homogeneously spread bilayers were formed on pure PEG-DA hydrogels, which was attributed to the hydrogels open and irregular structure. Instead, lipid bilayer patches and intact vesicles were obtained throughout the hydrogel. The possibility to covalently anchor lipid bilayers to amine modified mesoporous and nonporous silica surfaces via fusion of tether containing vesicles initiated by AH peptides was demonstrated. Results showed that the bilayers were homogenously spread on the surfaces with a thickness of 6-7 nm on mesoporous silica and about 3-4 nm on nonporous silica.

The signal-to-noise ratio of the QCM-D signal was improved when mesoporous material was used as sensing surface. It was observed that both the pore size and the chemical composition of the material influenced the measurements. A larger signal was observed when the analytes were smaller than the pores and when they were chemically attracted to the material. However, analytes that had low affinity to a material were possible to detect by introducing pores in the material.

In summary, mesoporous materials are promising to use in biosensing and drug delivery applications due to its tunable properties, such as pore size, pore orientation, chemical composition and surface chemistry. A natural continuation of the project would be to develop a controlled way to insert transmembrane proteins in both the supported lipid bilayers and the tethered lipid bilayers to

investigate the impact the different systems have on the proteins. The mobility of the proteins and the transport of ions through the same should be evaluated. Also, the use of ordered PEG-DA hydrogel particles and tethered lipid bilayers on mesoporous particles as drug delivery vehicles would be of interest to further develop to create a system that provides a higher stability and larger loading capacity when compared to existing systems.

# Chapter 8

## Acknowledgement

The Swedish research council (VR 2008-3660) and the materials area of advance, Chalmers University of Technology, are acknowledged for the financial support of this project.

I would also like to thank the following people:

My supervisor **Martin Andersson**, for always being supportive, enthusiastic, creative, and curious about my work. I do really appreciate all valuable scientific discussions and chitchats we have had and most importantly that you gave me the opportunity to perform parts of my work at Stanford University and at Nanyang Technical University. I would also like to thank my co-supervisor, **Sofia Svedhem**, for all good advices.

My examiner, **Krister Holmberg**, for giving me the opportunity to do research at Applied Surface Chemistry.

My co-writers, **Rickard Frost, Hoda Mashadi Fathali, Kristin Engberg, Curtis W. Frank, Nam-Joon Cho, Annika Altskär, Lars Nordstierna, Seong Oh Kim** and **Jae Hyok Choi** for many fruitful discussions and especially for the fun time we had together.

My former diploma workers, **Akbar Ahmadi, Lars Sonesson** and **Hasan Can Helvaci** for contributing a lot to my project.

My roommates, **Philip Karlsson, Lars Nordstierna, Emma Westas** and **Jonatan Bergek** for all scientific and non-scientific chats. You have made my time at Applied Surface Chemistry unforgettable.

All colleagues for creating a nice and great atmosphere at the department during "fika", lunches, courses and conferences. Especially thanks to **Hanna, Johan, Wenxiao "Chlor", Simon, Maria P., Alexander, Caroline, Sanna, Johanna,**

**Romain, Alireza, Rickard "Ralf", Christoffer**, **Markus, Björn, Frida, Sanna, Marina, Negin** and **Moheb**, Thanks to the innebandy "crew" for all fun games.

People at biological physics for sharing your knowledge, curiosity and helpfulness. Especially thanks to **Peter Jönsson** and **Deborah Rupert** for all help in the FRAP lab.

Meinen lieben Mann und besten Freund, **Patric Wallin**. Danke, dass du immer für mich da bist und mich immer ruhig und glücklich machst. Du und unser wunderbarer Sohn, **Peter**, bedeuten alles für mich.

Finally lots of thanks to my family and friends for all your support and encouragement. Especially thanks to my wonderful sister **Julia Claesson** for always being there for me and supporting me in tough and easy times.

# Chapter 9

## References


[1] J. Rouquerol, D. Avnir, C. W. Fairbridge, D. H. Everett, J. H. Haynes, N. Pernicone, J. D. F. Ramsay, K. S. W. Sing and K. K. Unger. Pure Appl. Chem. 1994, 66, 1739-1758.

[2] J. E. R. Vincent Chiola, Clarence D. Vanderpool, Process for producing low-bulk density silica US 3556725D A, 1971.

[3] R. B. Madeleine LE Page, Jacques Duchene, Porous silica particles containing a crystallized phase and method US 3493341D A 1967.

[4] G. K. Hanns Biegler, Process for producing silica in the form of hollow spheres. US 342525 A 1964.

[5] C. T. Kresge, M. E. Leonowicz, W. J. Roth, J. C. Vartuli and J. S. Beck. Nature 1992, 359, 710-712.

[6] M. Vallet-Regi, M. Colilla and I. Izquierdo-Barba. J. Biomed. Nanotech. 2008, 4, 1-15.

[7] M. Manzano, M. Colilla and M. Vallet-Regi. Expert Opinion on Drug Delivery 2009, 6, 1383-1400.

[8] M. A. Vallet-Regi, L. Ruiz-Gonzalez, I. Izquierdo-Barba and J. M. Gonzalez-Calbet. J. Mater. Chem. 2006, 16, 26-31.

[9] S. Baskaran, J. Liu, K. Domansky, N. Kohler, X. H. Li, C. Coyle, G. E. Fryxell, S. Thevuthasan and R. E. Williford. Adv. Mater. 2000, 12, 291-294.

[10] H. Y. Fan, H. R. Bentley, K. R. Kathan, P. Clem, Y. F. Lu and C. J. Brinker. J. Non-Cryst. Solids 2001, 285, 79-83.

[11] G. Wirnsberger, B. J. Scott and G. D. Stucky. Chem. Commun. 2001, 119-120.

[12] P. Innocenzi, A. Martucci, M. Guglielmi, A. Bearzotti and E. Traversa. Sensors and Actuators B. 2001, 76, 299-303.

[13] M. Klotz, A. Ayral, C. Guizard and L. Cot. Sep. Purif. Technol. 2001, 25, 71-78.

[14] P. D. Yang, G. Wirnsberger, H. C. Huang, S. R. Cordero, M. D. McGehee, B. Scott, T. Deng, G. M. Whitesides, B. F. Chmelka, S. K. Buratto and G. D. Stucky. Science 2000, 287, 465-467.

[15] S. Besson, T. Gacoin, C. Ricolleau, C. Jacquiod and J. P. Boilot. Nano Lett. 2002, 2, 409-414.

[16] K. Holmberg. J. Colloid Interface Sci. 2004, 274, 355-364.

[17] M. Andersson, H. M. Keizer, C. Y. Zhu, D. Fine, A. Dodabalapur and R. S. Duran. Langmuir 2007, 23, 2924-2927.

[18] M. Andersson, G. Okeyo, D. Wilson, H. Keizer, P. Moe, P. Blount, D. Fine, A. Dodabalapur and R. S. Duran. Biosens. Bioelectron. 2008, 23, 919-923.

[19] S. Ganta, H. Devalapally, A. Shahiwala and M. Amiji. J. Controlled Release 2008, 126, 187-204.

[20] M. J. H. Pieter R. Cullis, editor Physical properties and functional roles of lipids in membranes. In: Vance DE, Vance JE (eds) Biochemistry of lipids and membranes. Benjammin/Cummings Pub. Co., 1985.

[21] R. P. Richter, R. Berat and A. R. Brisson. Langmuir 2006, 22, 3497-3505.

[22] M. Tanaka and E. Sackmann. Nature 2005, 437, 656-663.

[23] M. Vallet-Regí and F. Balas. The Open Biomedical Engineering Journal 2008, 2, 1-9.

[24] J. Karlsson, R. Jimbo, H. M. Fathali, H. O. Schwartz, M. Hayashi, M. Halvarsson, A. Wennerberg and M. Andersson. Acta Biomater. 2012, 8, 4438-4446.

[25] D. Myung, W. Koh, A. Bakri, F. Zhang, A. Marshall, J. M. Ko, J. Noolandi, M. Carrasco, J. R. Cochran, C. W. Frank and C. N. Ta. Biomed. Microdevices 2007, 9, 911-922.

[26] D. Myung, W. U. Koh, J. M. Ko, Y. Hu, M. Carrasco, J. Noolandi, C. N. Ta and C. W. Frank. Polymer 2007, 48, 5376-5387.

[27] R. M. K. Ramanan, P. Chellamuthu, L. P. Tang and K. T. Nguyen. Biotechnol. Progr. 2006, 22, 118-125.

[28] M. Luckey. Membrane structural biology whit biochemical and biophysical foundations. New York: Cambridge University prss, 2008.

[29] W. F. Boron, Boulpaep, E. L., Medical Physiology: A cellular and molecular approach. Philadelphia, PA: Elsevier Inc., 2009.

[30] L. K. Tamm and H. M. McConnell. Biophys. J. 1985, 47, 105-113.

[31] P. Jonsson, M. P. Jonsson, J. O. Tegenfeldt and F. Hook. Biophys. J. 2008, 95, 5334-5348.

[32] S. J. Singer and G. L. Nicolson. Science 1972, 175, 720-731.

[33] A. A. Brian, McConnell, H. M. Proc. Natl. Acad. Sci. 1984, 81, 6159-6163.

[34] D. D. Chiras, Human Biology. Canada: Jones and Bartlett publisher, LLC, 2009.

[35] D. Keizer M H, R B Andersson M, Fine D, Price B R, Long R J, Dodabalapur A, Köper I, Knoll W, Anderson A V P and Duran S R. ChemBioChem 2007, 8, 1246-1250.

[36] E. K. Schmitt, M. Nurnabi, R. J. Bushby and C. Steinem. Soft Matter 2008, 4, 250-253.

[37] E. Sackmann. Science 1996, 271, 43-48.

[38] K. C. Weng, J. J. R. Stalgren, S. H. Risbud and C. W. Frank. 7th International Symposium on Aerogels. Alexandria, VA: Elsevier Science Bv, 2003. 46-53.

[39] M. P. Jonsson, P. Jonsson, A. B. Dahlin and F. Hook. Nano Lett. 2007, 7, 3462-3468.

[40] P. Jonsson, M. P. Jonsson and F. Hook. Nano Lett. 2010, 10, 1900-1906.

[41] O. Worsfold, N. H. Voelcker and T. Nishiya. Langmuir 2006;22:7078-7083.

[42] F. Cunin, P. E. Milhiet, E. Anglin, M. J. Sailor, C. Espenel, C. Le Grimellec, D. Brunel and J. M. Devoisselle. Ultramicroscopy 2007, 107, 1048-1052.

[43] I. Pfeiffer, S. Petronis, I. Koper, B. Kasemo and M. Zach. J. Phys. Chem. B. 2010, 114, 4623-4631.
[44] J. McMurry, Fundamentals of Organic Chemistry. Pacific Grove, CA: Brooks/Cole, 2003.
[45] G. Nordlund, J. B. S. Ng, L. Bergstrom and P. Brzezinski. Acs Nano 2009, 3, 2639-2646.
[46] J. W. Liu, A. Stace-Naughton, X. M. Jiang and C. J. Brinker. J. Am. Chem. Soc. 2009, 131, 1354-1355.
[47] S. Mornet, O. Lambert, E. Duguet and A. Brisson. Nano Lett. 2005, 5, 281-285.
[48] C. Rossi and J. Chopineau. Eur. Biophys. J. Biophys. Lett. 2007, 36, 955-965.
[49] B. J. Melde and B. J. Johnson. Anal. Bioanal. Chem. 2010, 398, 1565-1573.
[50] B. J. J. Melde, B. J.and Charles, P. T. Sensors 2008, 8, 5202-5228.
[51] J. Andersson, J. Rosenholm, S. Areva and M. Linden. Chem. Mater. 2004, 16, 4160-4167.
[52] S. Oh, J. Moon, T. Kang, S. Hong and J. Yi. Sensors and Actuators B. 2006, 114, 1096-1099.
[53] A. Palaniappan, X. Li, F. E. H. Tay, J. Li and X. D. Su. Sensors and Actuators B. 2006, 119, 220-226.
[54] B. Ji and H. Gao. Ann. Rev. Mater. Res. 2010, 40, 77-100.
[55] H. J. Choi and S. S. Ray. J. Nanosci. Nanotechnol. 2011, 11, 8421-8449.
[56] S. Venkataraman, J. L. Hedrick, Z. Y. Ong, C. Yang, P. L. R. Ee, P. T. Hammond and Y. Y. Yang. Adv. Drug Deliv. Rev. 2011, 63, 1228-1246.
[57] D. A. Cardoso, J. A. Jansen and S. C. G. Leeuwenburgh. J. Biomed. Mater. Res. Part B 2012, 100B, 2316-2326.
[58] M. Fujiki, J. Koe, K. Terao, T. Sato, A. Teramoto and J. Watanabe. Polym. J. 2003, 35, 297-344.
[59] H. Li and W. Huck. Curr. Opin. Solid State Mat. Sci. 2002, 6, 3-8.
[60] J. D. Clapper, L. Sievens-Figueroa and C. A. Guymon. Chem. Mater. 2008, 20, 768-781.
[61] K. J. Holmberg, Bo. Kronberg, Bengt. Lindman, Björn. Surfactants and polymers in aqueous solution. England, John Wiley & Sons, 2007.
[62] M. J. Rosen. Surfactant and Interfacial Phenomena. New York, Wiley, 2004.
[63] A. E. C. Palmqvist. Curr. Opin. Colloid Interface Sci. 2003, 8, 145-155.
[64] Y. F. Lu, R. Ganguli, C. A. Drewien, M. T. Anderson, C. J. Brinker, W. L. Gong, Y. X. Guo, H. Soyez, B. Dunn, M. H. Huang and J. I. Zink. Nature 1997, 389, 364-368.
[65] P. C. A. Alberius, K. L. Frindell, R. C. Hayward, E. J. Kramer, G. D. Stucky and B. F. Chmelka. Chem. Mater. 2002, 14, 3284-3294.
[66] R. G. Gennis and J. L. Strominger. J. Biol. Chem. 1976, 251, 1277-82.
[67] P. M. Kruglyakov, V. D. Mal'kov and T. P. Sedova. Colloid J. 2002, 64, 719-724.
[68] G. Morel. Handbook of Cryo-Preprataion Methods for Electron Microscopy. Taylor & Francis Group, LLC, 2009.
[69] R. G. Laughlin. The Aqueous Phase Behavior of Surfactants. Academic Press, 1994.

[70] S. E. Brunauer, P. H.; Teller, E. J. J. Am. Chem. Soc. 1938, 60, 309-319.
[71] E. P. Barrett, L. G. Joyner and P. P. Halenda. J. Am. Chem. Soc. 1951, 73, 373-380.
[72] O. L. Söderman, B. . Surfactant Sci. Ser. 2005, 213-240.
[73] M. J. Hope, M. B. Bally, G. Webb and P. R. Cullis. Biochim. Biophys. Acta 1985, 812, 55-65.
[74] E. Reimhult, F. Hook and B. Kasemo. Langmuir 2003, 19, 1681-1691.
[75] C. A. Keller, K. Glasmastar, V. P. Zhdanov and B. Kasemo. Phys. Rev. Lett. 2000, 84, 5443-5446.
[76] J. A. Zasadzinski, R. Viswanathan, L. Madsen, J. Garnaes and D. K. Schwartz. Science 1994, 263, 1726-1733.
[77] R. C. Macdonald, R. I. Macdonald, B. P. M. Menco, K. Takeshita, N. K. Subbarao and L. R. Hu. Biochim. Biophys. Acta 1991, 1061, 297-303.
[78] E. Sackmann and M. Tanaka. Trends Biotechnol. 2000, 18, 58-64.
[79] E. K. Sinner and W. Knoll. Curr. Opin. Chem. Biol. 2001, 5, 705-711.
[80] G. Sauerbrey. Z. Phys. 1959, 155, 206-222.
[81] F. Hook, B. Kasemo, T. Nylander, C. Fant, K. Sott and H. Elwing. Anal. Chem. 2001, 73, 5796-5804.
[82] C. A. Keller and B. Kasemo. Biophys. J. 1998, 75, 1397-1402.
[83] D. Axelrod, D. E. Koppel, J. Schlessinger, E. Elson and W. W. Webb. Biophys. J. 1976, 16, 1055-1069.
[84] S. R. Cohen and A. Bitler. Curr. Opin. in Colloid Interface Sci. 2008, 13, 316-325.
[85] R. J. Colton, D. R. Baselt, Y. F. Dufrene, J. B. D. Green and G. U. Lee. Curr. Opin. Chem. Biol. 1997, 1, 370-377.
[86] M. Kaszuba, D. McKnight, M. T. Connah, F. K. McNeil-Watson and U. Nobbmann. J. Nanopart. Res. 2008, 10, 823-829.
[87] T. Coquil, E. K. Richman, N. J. Hutchinson, S. H. Tolbert and L. Pilon. J. Appl. Phys. 2009, 106,11.
[88] S. Besson, T. Gacoin, C. J. Ricolleau, C. and J.-P. Boilot. J. Mater. Chem. 2003, 13, 404-409.
[89] P. Alexandridis, U. Olsson and B. Lindman. Langmuir 1998, 14, 2627-2638.
[90] D. J. Waters, K. Engberg, R. Parke-Houben, L. Hartmann, C. N. Ta, M. F. Toney and C. W. Frank. Macromolecules 2010, 43, 6861-6870.
[91] J. D. Clapper and C. A. Guymon. Macromolecules 2007, 40, 1101-1107.
[92] B. S. Forney and C. A. Guymon. Macromolecules 2010, 43, 8502-8510.
[93] C. L. Lester, C. D. Colson and C. A. Guymon. Macromolecules 2001, 34, 4430-4438.
[94] M. Claesson, K. Engberg, C. W. Frank and M. Andersson. Soft Matter 2012, 8, 8149-8156.
[95] B. J. Boyd, S. B. Rizwan, Y. D. Dong, S. Hook and T. Rades. Langmuir 2007, 23, 12461-12464.
[96] J. Gustafsson, T. Nylander, M. Almgren and H. Ljusberg-Wahren. J. Colloid Interf. Sci. 1999, 211, 326-335.
[97] R. Richter, A. Mukhopadhyay and A. Brisson. Biophys. J. 2003, 85, 3035-3047.

[98] R. P. Richter and A. R. Brisson. Biophys. J. 2005, 88, 3422-3433.
[99] I. Reviakine, F. F. Rossetti, A. N. Morozov and M. Textor. J. Chem. Phys. 2005, 122, 8.
[100] A. Wikstrom, S. Svedhem, M. Sivignon and B. Kasemo. J. Phys. Chem. B. 2008, 112, 14069-14074.
[101] J. Solon, P. Streicher, R. Richter, F. Brochard-Wyart and P. Bassereau. Proceedings of the National Academy of Sciences of the US 2006, 103, 12382-12387.
[102] A. R. Sapuri, M. M. Baksh and J. T. Groves. Langmuir 2003, 19, 1606-1610.
[103] A. Kunze, S. Svedhem and B. Kasemo. Langmuir 2009, 25, 5146-5158.
[104] M. C. Claesson, N-J. Frank, C W. Andersson, M. Langmuir 2010, 26, 16630–16633.
[105] E. Reimhult, F. Hook and B. Kasemo. J. Chem. Phys. 2002, 117, 7401-7404.
[106] H. M. Seeger, A. Di Cerbo, A. Alessandrini and P. Facci. J. Phys. Chem. B 2010, 114, 8926-8933.
[107] N. J. Cho and C. W. Frank. Langmuir 2010, 26, 15706-15710.
[108] N.-J. Cho, Jackman, J. A., Liu, M., and Frank, C. W., . Langmuir 2011, 27, 3739-3748.
[109] F. F. Rossetti, M. Bally, R. Michel, M. Textor and I. Reviakine. Langmuir 2005, 21, 6443-6450.
[110] F. F. Rossetti, M. Textor and I. Reviakine. Langmuir 2006, 22, 3467-3473.
[111] D. Y. Zhao, J. L. Feng, Q. S. Huo, N. Melosh, G. H. Fredrickson, B. F. Chmelka and G. D. Stucky. Science 1998, 279, 548-552.
[112] C. Rossi, J. Homand, C. Bauche, H. Hamdi, D. Ladant and J. Chopineau. Biochemistry 2003, 42, 15273-15283.
[113] V. Atanasov, N. Knorr, R. S. Duran, S. Ingebrandt, A. Offenhausser, W. Knoll and I. Koper. Biophys. J. 2005, 89, 1780-1788.
[114] A. Junghans and I. Koper. Langmuir 2010, 26, 11035-11040.
[115] S. Kaufmann, G. Papastavrou, K. Kumar, M. Textor and E. Reimhult. Soft Matter 2009, 5, 2804-2814.
[116] N. J. Cho, K. H. Cheong, C. Lee, C. W. Frank and J. S. Glenn. J. Virology 2007, 81, 6682-6689.
[117] B. Adhikari and S. Majumdar. Prog. Polym. Sci. 2004, 29, 699-766.
[118] www.dendritech.com, 10 Dec 2011